CODEN:LUTEDX/(TEIE-5493)/1-64/(2023)

Industrial Electrical Engineering and Automation

Network reconfiguration for renewable generation maximization

Application of a power-flow optimization algorithm on a distribution network in southern Sweden

Gabriel Malmer
Lovisa Thorin

Division of Industrial Electrical Engineering and Automation
Faculty of Engineering, Lund University

Gabriel Malmer och Lovisa Thorin
Avdelningen för industriell elektroteknik och automation
Juni 2023

Populärvetenskaplig sammanfattning

Nätomkoppling för att maximera lokal förnybar elproduktion

Om det befintliga elnätet kopplas om kan mer lokal elproduktion tas upp. Användning av optimering med nätomkoppling kan hjälpa operatörer att hitta bättre nätstrukturer för detta ändamål. Metoden är kostnadseffektiv och visar lovande resultat.

För att bekämpa klimatförändringarna krävs att fossila bränslen fasas ut snarast. Många av de sektorer som idag drivs fossilt har goda möjligheter att drivas av el från förnybara källor som sol och vind i framtiden. För det krävs dock en ökad elproduktion från dessa källor, och att vi har ett elnät som kan ta emot och fördela den kraft som produceras. Idag installeras mer och mer solceller på hustak och lokala vindkraftverk blir allt vanligare, men distributionsnäten är sällan konstruerade för att ta emot stora mängder lokal elproduktion. Begreppet *värdkapacitet* används för att bestämma mängden effekt som ett distributionsnät kan ta emot och fördela. I en perfekt värld skulle alla nät ha oändlig värdkapacitet, men i praktiken finns det flera faktorer som begränsar den – till exempel hur hög strömmen får vara och hur mycket spänningen får variera i nätet. När värdkapaciteten är nådd måste elproduktionen minska, alternativt måste nya kraftverk stoppas från att ansluta till nätet.

Många distributionsnät i Sverige är byggda i en maskad struktur, alltså med slutna slingor och minst två möjliga vägar till varje nätstation. Samtidigt drivs de flesta distributionsnät idag radiellt för feldetektering och enklare koordination av skyddssystemen, vilket innebär att det bara finns en aktiv väg till varje station. Det innebär att vissa ledningar i nätet hålls inaktiva, och att dessa bara aktiveras om det sker ett fel och omkoppling krävs.

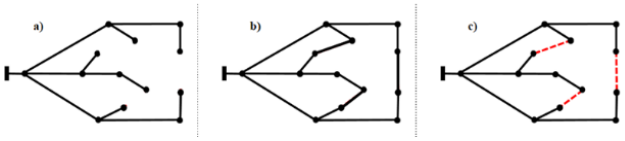

Bild a) visar ett radiellt nät. Bild b) visar ett maskat nät. Bild c) visar ett maskat nät som drivs radiellt (röda linjer är inaktiva ledningar).

Vilka ledningar som är aktiva respektive inaktiva kan bestämmas av systemoperatören, genom att slå av och på brytare i nätstationerna. Att utföra sådana omkopplingar, och alltså ändra vilka ledningar som är aktiva, kallas för *nätomkoppling*. Nätomkoppling är en teknik som kan användas för att öka värdkapaciteten i elnätet. Genom att koppla nätet så att elproduktionen fördelas på olika ledningar, och på de som är bäst lämpade för att ta emot stora effektflöden i det givna fallet, kan värdkapaciteten öka.

I det här examensarbetet har vi arbetat med en optimeringsalgoritm som maximerar lokal elproduktion för ett givet förbrukningsfall, med begränsningar på exempelvis ström och spänning. Samtidigt tillåter algoritmen nätomkopplingar, så att den tar fram den kopplingsstruktur av nätet som ger maximal värdkapacitet i det givna fallet. Algoritmen är utvecklad av en forskare i Taiwan, men var tidigare bara testad på standardmodeller av mindre elnät. Vi har byggt en större och mer detaljerad modell av ett verkligt distributionsnät i södra Sverige (Eslöv) och kört algoritmen på denna. Genom att i modellen placera ut elproduktion och köra optimeringen kan vi se hur stor värdkapaciteten är på olika platser i nätet, och hur stor nytta nätomkoppling kan göra för att öka den.

Våra resultat visar att nätomkoppling med så få som fyra omkopplingar kan leda till en tredubbling i värdkapacitet på specifika platser i nätet. Resultaten varierar dock kraftigt beroende på var i nätet elproduktion installeras, och på vissa platser hade nätomkoppling nästan ingen inverkan alls. Det är också viktigt att analysera de nätomkopplingar som har gjorts, så att inte instabila kopplingsstrukturer skapats.

Vår slutsats är att nätomkoppling är ett bra verktyg för att öka mängden förnybar energi som kan installeras i lokala elnät – speciellt eftersom metoden är billig och snabbt går att ta i bruk jämfört med att bygga nya ledningar vilket ofta är både dyrt och tidskrävande. Optimering med nätomkoppling kan användas som beslutsstöd av nätbolag för att hitta nya kopplingsstrukturer med högre värdkapacitet som annars eventuellt hade förbisetts.

Network reconfiguration for renewable generation maximization

Application of a power-flow optimization algorithm
on a distribution network in southern Sweden

Gabriel Malmer & Lovisa Thorin

A thesis presented for the degree of
Masters of Science in Engineering Physics

LUNDS
UNIVERSITET

Division of Industrial Electrical Engineering and Automation (LTH)
Lund University, May 2023
Supervisor: Professor Olof Samuelsson
Examiner: Morten Hemmingsson

All models are wrong,
but some are useful.

GEORGE E.P. BOX

Preface

An ambition for this thesis, beside the actual research objectives, was to explore the world in between academia and operation. This is the space where many power systems engineers work, trying to bridge the gap between the interdisciplinary, forward-thinking researchers and the more hands-on, skillful operators of electrical systems. In this unofficial goal, we believe to have succeeded, at least to the extent one can expect over the span of a semester. This is partly because of the work we have done, but mainly due to all the helpful contacts we have had – enabling us to connect not only academia and operation but also Eslöv and Taiwan.

We would really like to thank Håkan Skarrie and Andreas Vikström from Kraftringen for their help in supplying us with (a lot of) necessary grid data, and along the way being helpful and willing to discuss the possibilities and limitations that exist when trying to model the real world.

Also a huge thank you to professor Kin Cheong Sou, for supplying us with a fantastically well documented and elegantly produced algorithm and code, and for putting up with late-night video calls between Sweden and Taiwan.

Lastly, we are very grateful to our supervisor Olof Samuelsson. For all your help and ingenious comments, for our fun and interesting meetings, and for being the one to introduce us to the world of power systems in the first place.

Division of Industrial Electrical Engineering and Automation
Faculty of Engineering
Lund University
Lund 2023

Abstract

Increasing the amount of renewable generation in distribution networks is a fundamental part of the energy transition. Multiple methods exist to increase the hosting capacity in a grid, to allow larger injections of generation and more efficiently utilize existing infrastructure before operational limits are breached. In this thesis, the method studied for this is network reconfiguration. Many distribution networks are built in a meshed structure but operated radially to allow the use of simple overcurrent protection. By closing and opening sectionalizing switches, new radial topologies can be found which enable a higher injection of distributed generation. In this work, optimal configurations for increased hosting capacity were found using a joint reconfiguration-optimal power flow algorithm. This was applied to a power flow model of a real 12 kV distribution network in southern Sweden, with 533 nodes and 45 tie switches. The results show that the reconfiguration optimization algorithm performs as intended and can be applied as decision support by a DSO to find new static, potentially overlooked, configurations. The relative increase in hosting capacity can be over 200% in certain scenarios, but large variations exist depending on time and location of the connections. To apply the algorithm in an automated and dynamic mode, robustness issues have to be addressed and grid adjustments made.

Keywords: Distributed generation, hosting capacity, network reconfiguration, optimal power flow, power distribution, optimization, mixed-integer programming

List of abbreviations

AC - Alternating Current

CHP - Combined Heat and Power

DC - Direct Current

DG - Distributed Generation

DSO - Distribution System Operator

HC - Hosting Capacity

HF - Hurva Fördelningsstation

HV - High Voltage

LF - Löberöd Fördelningsstation

LV - Low Voltage

MF - Marieholm Fördelningsstation

MIP - Mixed Integer Problem

MV - Medium Voltage

OHL - Overhead Line

OPF - Optimal Power Flow

PV - Photovoltaics

PF - Power Flow

RMU - Ring Main Unit

R-OPF - Reconfiguration-Optimal Power Flow

SP - Södra Primärstationen

TSO - Transmission System Operator

ÖP - Östra Primärstationen

List of variables

α_{ij} - Binary variable defining if node i is connected to node j.

α_{ij}^{0} - Binary variable defining if node i is connected to node j in the normal configuration.

C - Apparent power rating of generator/inverter.

$c(i)$ - The set of all nodes which have node i as its parent bus.

δ_i - Voltage phase angle at node i.

ΔV - Voltage magnitude difference between two connected nodes.

f_{ij} - Continuous auxiliary flow variable between nodes i and j, ensuring network connectedness.

K - Allowed number of switch events from the normal configuration.

ℓ_i - Squared line current towards node i, measured at the parent node (π_i).

$\overline{\ell}$ - Squared line current upper limit (rated current squared).

$\mathcal{N}$ - The set of all nodes in the system, excluding the slack bus.

$\bar{\mathcal{N}}$ - The set of all nodes in the system, including the slack bus.

N - Number of nodes in the system, excluding the slack bus.

ν_i - Squared voltage magnitude at node i.

ν_{π_i} - Squared voltage magnitude at the parent node (π_i) of node i.

$\underline{\nu}$ - Squared voltage magnitude lower limit.

$\overline{\nu}$ - Squared voltage magnitude upper limit.

P_i - Active power flow towards node i, measured at the parent node (π_i).

P_i^{LF} - Active power injection at node i (*Load Flow*).

p_i^G - Active power injection at node i from distributed generation.

p_i^L - Active power load at node i.

pf - Power factor of generator/inverter.

pf_{min} - Power factor lower limit of generator/inverter.

π_{ij} - Binary variable defining if node i is parent to node j.

Q_i - Reactive power flow towards node i, measured at the parent node (π_i).

Q_i^{LF} - Reactive power injection at node i (*Load Flow*).

q_i^G - Reactive power injection at node i from distributed generation.

q_i^L - Reactive power load at node i.

r_i - Resistance of the active line between node i and the parent node (π_i).

r_{ij} - Resistance of the line between nodes i and j.

S_{ij} - Apparent power flow leaving node i towards node j.

θ_{ij} - Admittance phase angle of the line between nodes i and j.

V_i - Voltage magnitude at node i.

V_{nom} - Nominal voltage magnitude of the system.

x_i - Reactance of the active line between node i and the parent node (π_i).

x_{ij} - Reactance of the line between nodes i and j.

$\bar{Y}_{ij}$ - Complex admittance of the line between nodes i and j.

$\bar{Z}_{ij}$ - Complex impedance of the line between nodes i and j.

Contents

Chapter 1

Introduction

To begin with, a general background to the issue of limited hosting capacity is presented in section 1.1, along with a review of previous research in the field in section 1.2. Then, going into the specifics of this project, the problem statement, aim of research and objectives of the thesis are presented in sections 1.3-1.5. The specific scope of the project is discussed in section 1.6. Finally, some of the terminology used in this paper is explained in section 1.7.

1.1 Background

Electric power is a flexible and scalable energy carrier with the potential to replace fossil fuels in many cases. In order to combat climate change while ensuring high standard of living, sectors that are run on fossil fuels today will need to be electrified and supplied with energy from renewable sources. An important part of this energy transition and electrification is the ongoing and projected increase of distributed generation (DG), such as solar and wind power. Not only are wind and solar renewable, but they have also become competitive in terms of levelized cost of electricity. Seeing the need for low-cost fossil-free electricity, it would be ideal if the electrical grid had the ability to receive and transfer any given amount of produced renewable power. In reality however, the grid has physical constraints that limit the possible uptake. This upper limit on how much generation a grid can accept is referred to as the hosting capacity (HC) of the grid [1]. Increased HC is desired in most systems, in order to permit connection of future DG units. This increase can be accomplished through different means, and is a relatively well researched field. Naturally, higher HC can be achieved by expansion or reinforcement of the grid, such as adding additional lines or upgrading to conductors with higher rated currents. But such investments are often both costly and time consuming. It is therefore of interest to find methods of increasing the HC without having to place large infrastructure investments, and instead utilize the existing grid infrastructure more efficiently. One such method is *reconfiguration of radial networks*, which is analyzed in depth in this thesis.

1.2 Literature review

Much of this project is based on the work by professor Kin Cheong Sou from the National Sun Yat-sen University in Taiwan. His paper *Joint Renewable Generation Maximization and Radial Distribution Network Reconfiguration* [2] outlines the mathematical details and the reconfiguration optimization algorithm used in this thesis. The novelty of his work lies in the usage of nonlinear DistFlow-equations in a joint reconfiguration and optimal power flow (R-OPF) problem. The validity of the method is proven in the paper using standard network test cases [2].

There is much previous research done targeted at finding methods for increasing the HC in distribution networks. Such methods include voltage control, as can be seen in [3] where tap-changers are used to control voltage locally, thereby allowing for a higher HC. In [4] HC enhancement is discussed through methods of increasing conductor cross sections (i.e. reinforcement of the grid)

to permit higher currents, and through installation of shunt reactances in the network. Authors in [5] and [6] analyze how active power curtailment can be used to increase HC. Comprehensive overviews of the research done and methods used to increase HC can be found in [7] and [8].

A few papers can be found which use reconfiguration to increase the HC. The papers [9] from 2005 and [10] from 2013 both use genetic algorithms applied on reconfiguration to increase integration/penetration of DG in distribution systems. In [11] the objective is loss minimization instead, but the sizing and placement of DG is a variable parameter. Though increased HC is not the objective of the algorithm, the authors state that they hope this approach will lead to "obtaining the maximum potential benefits of these [DG] units". In [12] from 2015, Capitanescu et al. present research similar to that done by Sou [2]: setting up a joint R-OPF problem with almost identical constraints and objective. The main difference between the two is the problem formulations. Capitanescu et al. use standard load flow equations whereas Sou applies DistFlow. Although radiality is demanded in both papers, it is enforced in different ways.

Using reconfiguration to improve HC has been looked at for some time, but is a relatively unexplored method compared to others. Within the field of network reconfiguration optimization, the objective is most often minimization of active power losses or maximization of some reliability index. Many papers in this field focus on the different optimization algorithms that can be used to perform the mixed-integer programming (MIP) optimization, including the particle swarm algorithm [13], the parallel slime mould algorithm [14], genetic algorithms [15] and hybrid combinations of other algorithms [16] – all with either the single objective of loss minimization or a joint objective of loss reduction and voltage control in some form.

1.3 Problem statement

Distribution networks are often built in a looped structure for redundancy but operate radially (with an open point) for simple and effective coordination of their protection systems [17, 18]. Consequently, the network has both sectionalizing lines (normally connected) and tie lines (normally disconnected). By disconnecting some of the connected lines and vice versa, the configuration of the network can be altered without losing the radial structure – a binary reconfiguration problem. Meanwhile, the standard optimal power flow (OPF) problem with arbitrary objective function only works on fixed configurations. By combining these two problems, the OPF problem for DG maximization can be expanded to a MIP problem that also takes reconfiguration into account, a problem which will be referred to as the R-OPF.

1.4 Aim of research

The aim of research is to increase the level of knowledge regarding network reconfiguration optimization, and study how it can be applied as a method to more efficiently utilize existing electrical grid infrastructure. By performing a case study on the distribution network in Eslöv with surroundings (a municipality in southern Sweden), the goal is to identify and discuss to which extent network reconfiguration can be a viable HC enhancement technique. The approach in this study is deterministic, as all loads and installed generation capacities in the system are assumed to be known for a set of defined scenarios. The intention is to demonstrate scenarios in which reconfiguration can be used as a method to increase HC, rather than to deal with probabilistic methods such as stochastic programming [19]. To achieve this, the following research objectives are defined:

1.5 Research objectives

1. Build an accurate power flow model of the distribution network in Eslöv with surroundings.
2. Apply the optimization algorithm developed by Sou to the model [2].
3. Quantify the increase of distributed generation in a set of defined scenarios.
4. Find general traits of the optimization algorithm.
5. Assess the robustness of the new configurations (post-optimization).
6. Suggest improvements to the algorithm to make it more applicable to real networks.

1.6 Scope and delimitations

The scope of this project can be described by its "task" and "tool". The *task* we want to accomplish is maximization of HC, in contrast to other tasks (objective functions) such as loss minimization or reliability maximization. The *tool* we are using is reconfiguration of networks, in contrast to other tools (HC enhancement techniques) such as cable reinforcement, reactive power control or energy storage.

A fundamental delimitation of the method used in this project is that only radially operated networks are considered. With a network in meshed operation, the recursive DistFlow equations used as constraints in the optimization model can not be applied. Furthermore, there is no obvious need to disconnect lines if meshed operation is possible, so the reconfiguration problem in itself becomes irrelevant.

Geographically, the data material studied is limited to the distribution network in Eslöv with surroundings. Timewise, all load and generation data is from the year 2022.

The HC operational limits enforced in this project are voltage and current limits. Protection is implicitly included by forcing the system to be radially operated, but no further study of protection is made. The system is assumed to be three-phase balanced and in steady-state normal operation. Harmonics are not studied.

1.7 Terminology

Throughout this project the use of certain terms may seem unclear, partly due to the wide scope, and we wish to clarify this early on. The majority of the work is very power systems related, with all the language included in that field, but some of the network modeling is closely related to graph theory and optimization, which carries its own terminology. The "nodes" in the network are electrically bus-bars or "buses". The "branches" are in power systems more commonly referred to as "lines", and are in reality conductors. These words will be used interchangeably throughout the text. The words "network", "grid" and "system" will be used as synonyms as well, when discussing the entire modeled electrical structure. In addition, the word "topology" will be used as equivalent to "configuration" when describing the layout of active and inactive lines in the network. Finally, in this paper no clear distinction is made between "looped" and "meshed" networks.

Chapter 2

Theory

First in this chapter, some basic information about power distribution systems, and the Swedish system in particular, will be covered in section 2.1. Section 2.2 explains the concept of hosting capacity in depth, and sections 2.3 and 2.4 go into the physical and mathematical details of power flow analysis and optimization thereof. Finally, sections 2.5 and 2.6 explain reconfiguration and how the joint optimization algorithm is formulated.

2.1 Electric power distribution

The three pillars of the electric power system are supply (generation), transfer, and consumption (load) of electric power. Transfer from generators to loads is carried out by conductors, i.e. cables or overhead lines (OHL), that together constitute the grid on each voltage level. The grid can be divided into two subsystems – the *transmission system* that carries large quantities of power at high voltages from generation hubs (large-scale production sites) to load hubs (transmission substations and large industries), and the *distribution system* that carries smaller quantities of power at lower voltages from hubs to individual consumers, producers and prosumers (homes, workplaces, smaller industries and distributed generation). Distributed generation (DG) is defined as electricity generated by small, often renewable, energy units that are connected to the medium voltage (MV) or low voltage (LV) distribution system. This in contrast to larger centralized production units, often nuclear, hydro or fossil-based, that connect to the high voltage (HV) transmission system.

In Sweden, the transmission system operates mainly at a voltage of 400 kV, with some smaller parts at 220 kV. The transmission system is administered and developed by the state-owned transmission system operator (TSO) Svenska kraftnät. A lower voltage level subtransmission system is connected to the transmission system, that transfers power to the even lower voltage distribution system. The subtransmission system in Sweden consists of regional grids (regionnät), usually operated at a voltage of 130 kV [20]. These are owned and operated by three large grid companies – Vattenfall, E.ON and Ellevio. In southern Sweden, where the case study for this thesis is located, the regional grid company is E.ON. Below the subtransmission system, the distribution system can be divided into a primary distribution system that operates at voltages below 40 kV, and a secondary distribution system that operates at the 400 V (230 V line-to-neutral) household voltage [20]. The primary distribution system delivers power between primary substations (primärstationer) and secondary substations (nätstationer), whereas the secondary distribution system delivers power between secondary substations and customers. The distribution system in Sweden consists of local grids (lokalnät). These are owned and operated by several different companies, referred to as distribution system operators (DSO:s). The DSO of the network in Eslöv used as case study in this thesis is Kraftringen. A schematic figure of the Swedish electrical grid can be seen in figure 2.1.

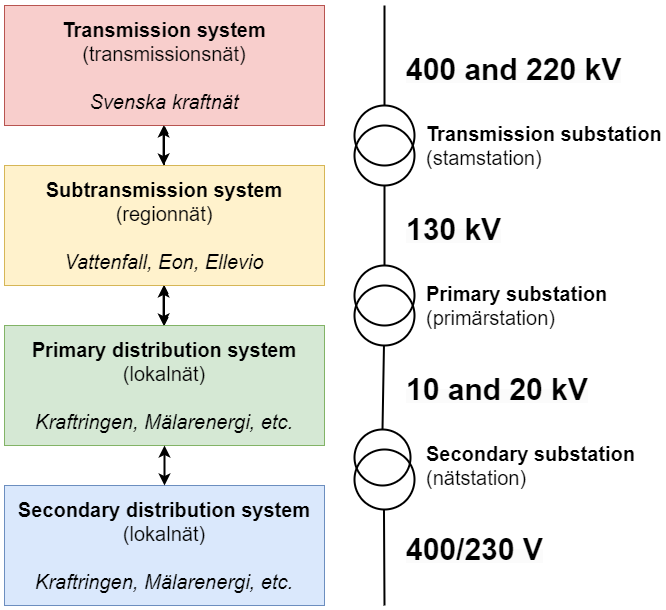

Figure 2.1: *Schematic figure of the Swedish electrical grid. The voltages are typical examples for the four subsystems in Sweden. 230 V in the secondary distribution system is the line-to-neutral voltage, all other voltage values are three-phase line-to-line.*

The study in this thesis is limited to the primary distribution system and a small part of the subtransmission system (green and yellow sections in figure 2.1). The network used as case study in this thesis is described further in section 3.1.

2.1.1 Network topology

In graph theory, a *radial* network is defined as an undirected network where there is only one path between any two given nodes – the equivalent of a tree. The feed-in substation connected to the regional grid can be seen as the root of this tree, and will be modeled as a fixed voltage source.

For distribution systems there are three basic types of topology: radial, looped and interconnected [21]. The radial system has the lowest investment cost but is also the least reliable, usually found in non-critical, rural areas. In radial systems, each given geographical area is connected only to one feeder line originating from the primary substation. If a fault occurs in a radial system, all consumers downstream the fault on the radial feeder are affected. The looped system (also referred to as the ring main system) is slightly more expensive, usually used where high reliability is more important. In looped systems, each line loops around a load area to several substations and returns, either to the same primary substation it originated from or to another one. Consequently, loads can be fed from two directions and there is redundancy in the system. If a fault occurs somewhere in a looped system, switching can be performed to isolate the specific faulted line section and restore service to all nodes on the loop. For a simple example of radial and looped systems, see figure 2.2. The interconnected system (also referred to as the meshed system) is the most expensive but also has the highest reliability. This is the usual topology for transmission and subtransmission grids. In meshed systems, all loads are connected in a grid structure to many primary substations [21]. If a fault occurs in a meshed system, service is never interrupted as the faulted line can be disconnected. It is rarely used in primary or secondary distribution networks.

It should here be emphasized that both looped and meshed primary distribution systems are normally *operated* radially, with one or more open points (tie lines) [21, 22], although they are *constructed* with more than one path to each load. This helps with fault location and makes the protection systems cheaper and easier to coordinate. Disconnection of lines is done by opening switches within the substations. These switches are typically circuit breakers, mounted directly within the substation, or load break switches, often enclosed within a ring main unit (RMU) in

the substation [23, 24] An RMU is a factory produced enclosed set of switchgear, with the specific ability to connect the load to either or both of the incoming feeders in the loop [23]. It should also be noted that not all secondary substations have sectionalizing switches.

In the future, it might be viable to operate distribution loops without any open point [24]. With meshed or looped operation, all existing infrastructure can be utilized simultaneously which would improve the DG hosting capacity more than any radial configuration. This will be discussed further in chapter 5.

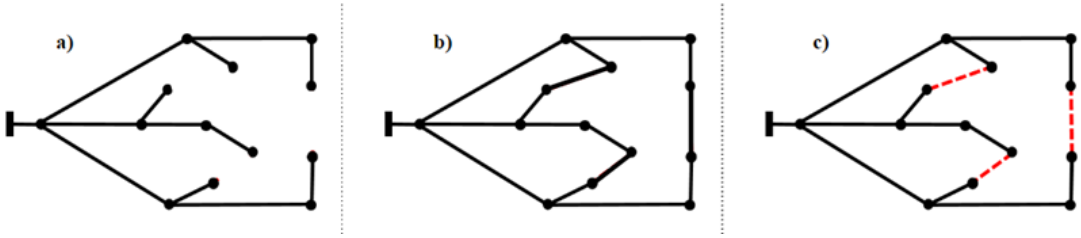

Figure 2.2: *Simple examples of layout structures. Figure a) shows a radial network. Figure b) shows a looped network. Figure c) shows a looped network that is operated radially, the red dashed lines represent tie lines.*

2.2 Hosting capacity

There are multiple ways of defining and discussing hosting capacity (HC). Most sources define HC as the amount of DG that can be integrated/added to a distribution network without any operational limits being breached [1, 7]. However, this still leaves room for two distinctly different categories of HC – snapshot and dynamic [1]. Snapshot HC is the traditional firm approach. It refers to the amount of generated power that can be *injected into the grid at a given time*. Studies of snapshot HC are usually based on some worst-case, static scenario such as the maximum or minimum load hour of the year. In contrast, dynamic HC refers to the possible power injection *over time*. Dynamic HC therefore also includes enhancement techniques such as active power curtailment and energy storage. These do not allow for higher injection to the grid when the grid is at its operational limits, but increase the amount of DG capacity that can reasonably be *connected to the grid*. This is discussed further in section 2.2.2.

In this thesis, focus lies on the snapshot HC – what the grid can accept at a given point in time. Furthermore, HC will refer to the total amount of power that can be injected *at nodes where additional DG is added*. As described in section 3.5, this is in some scenarios a single node, and in other scenarios it is over a hundred. Consequently, the magnitude of the HC differs widely between scenarios.

2.2.1 Operational limits

The operational limits that restrict HC are essentially voltage limits, current (thermal) limits, protection (short-circuit capacity) limits and harmonics (power quality) [7]. This project will mainly focus on the first two of these. As mentioned in section 1.6, protection is partly included by forcing the system to be radially operated, but no further study of protection is made. The system is assumed to be three-phase balanced and in steady-state normal operation.

For stable and secure operation of a power system, bus voltage magnitudes must stay close to the nominal voltage magnitude V_{nom} of the system. According to the European standard the 10 minute average root mean square voltage in low and medium voltage networks must stay within $\pm 10\%$ of V_{nom} for 95% of the time [25]. When designing the system for standard operation, it is common to require that bus voltages lay within $\pm 5\%$ of V_{nom} [2, 12, 17]. As a rule of thumb, the difference in voltage magnitude between two connected nodes (ΔV) is linearly proportional to the apparent power flow ($S = P + jQ$) and the impedance ($Z = R + jX$) of the line connecting the two nodes [7]:

$$\Delta V \cong \frac{(P \cdot R) + (Q \cdot X)}{V_{nom}} \tag{2.1}$$

This approximate relationship can also be derived from the DistFlow equivalent of Ohm's law, see equation (2.9). In other words, voltage variations increase with higher power flows and higher impedances (weaker lines). The voltage decreases in the direction of the power flow. In distribution grids, high load tends to cause low voltages while high DG tends to cause high voltages.

The rated current of a line is also a fundamental operational limit. If the current on a line exceeds the rated current, fuses and breakers might (and should) interrupt the circuit. If not, the line or other equipment is at risk of becoming too hot, thereby melting or in other ways being damaged. Consequently, current limits are often referred to as thermal limits.

2.2.2 Enhancement techniques

As previously touched upon, there are several techniques to the enhance HC in a distribution network. The most obvious one is expansion or reinforcement of the network, such as adding or upgrading to larger conductors. In doing so, rated currents can be increased and impedances decreased, thereby leaving room for more DG insertion before current and voltage limits are breached. Another important enhancement technique is improved voltage control. This can be done by introducing tap-changers in transformers or by increased reactive power control. Tap-changers allow the DSO to regulate the turns ratio of a transformer, thereby enabling control of the setpoint voltage at that node in the network [21]. Reactive power control can be done in synchronous generators and in inverters (PV and wind), but also with capacitor banks. In inverters, reactive power control is done by controlling the power factor of the inverter. This will act as a constraint in the optimization algorithm of this project and is discussed further in section 2.4.1. Reactive power control is considered one of the most promising methods to avoid overvoltage problems [7], and both tap-changing transformers and reactive power control have been proven effective methods to enhance HC, both over time and instantaneously [25]. A third technique for increasing the snapshot HC is to use reconfiguration and alter the topology of radially operated meshed networks. This is discussed further in section 2.5 and is the aim of this paper.

If the goal is to increase the dynamic HC, additional means are available. If power is not required to be injected to the grid instantaneously, energy storage (e.g. batteries) can be installed for depositing excess energy on-site during times when the network is otherwise "full" (at risk of overvoltages or overcurrents). This can then be injected at later occasions. Another dynamic enhancement technique is active power curtailment. If power producers agree to have generation curtailed, higher DG capacities can be installed in the grid and larger amounts of power can be injected at non-peak hours [7]. In figure 2.3, the concept of HC enhancement is visualized.

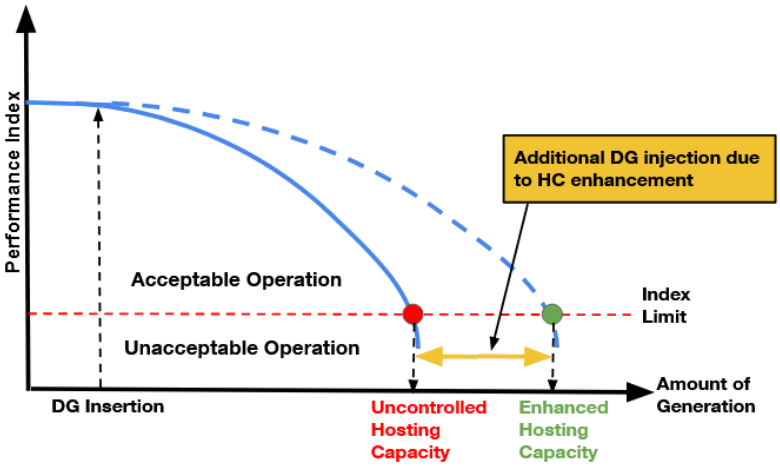

Figure 2.3: *Hosting capacity and the effect of enhancement. The Index Limit can be a current or voltage limit, or some other relevant constraint to the system, and the Performance Index is some measure of how far from this limit the system is operating. The figure is inspired by [7].*

2.3 Power flow analysis

For a power system to operate under normal balanced three-phase steady-state conditions, the following criteria are required [21]:

1. Generation supplies power to balance loads and losses.
2. Bus voltage magnitudes remain close to rated values.
3. Generators operate within their real and reactive power limits.
4. Lines and transformers are not overloaded.

The numerical analysis of these criteria is referred to as a power-flow (PF) study. For AC power systems, this analysis requires a set of nonlinear equations, containing bilinear and sometimes trigonometric terms. Thus even for smaller systems, computers with numerical solvers are normally used. The output of a PF computation is generally the complex voltages (in polar or cartesian coordinates) at each bus in the system. Based on this, other quantities such as real and reactive power flow on each line, currents, etc. can be calculated.

2.3.1 Load Flow and Newton-Raphson

One of the most common solution methods to the PF problem is the Newton-Raphson method. In this method, an admittance matrix $\mathbf{Y_{bus}}$ is created that mainly captures the impedance $\bar{Z_{ij}}$ of each line in the grid ($\bar{Z_{ij}} = 1/\bar{Y_{ij}}$). An $\mathbf{x}$ vector with voltage angle and magnitude (δ_i and V_i) at each bus is created and similarily a $\mathbf{y}$ vector with real and reactive power (P_i^{LF} and Q_i^{LF}) injected at each bus is created:

$$\mathbf{x} = \begin{bmatrix} \boldsymbol{\delta} \\ \mathbf{V} \end{bmatrix}, \quad \mathbf{y} = \begin{bmatrix} \mathbf{P} \\ \mathbf{Q} \end{bmatrix}$$

Each bus is assigned a type (PV, PQ or slack) based on which values are known and unknown respectively (PV = P and V known, PQ = P and Q known, slack (reference) = δ and V known). Thereafter, a representation of power physics must be included in the method. Equation (2.2) is the expression for apparent power flow on a line:

$$S_{ij} = \bar{V_i}\bar{I_i}^* = \bar{V_i}(\frac{\bar{V_i} - \bar{V_j}}{\bar{Z_{ij}}})^* \tag{2.2}$$

Since the complex voltage, admittance and apparent power can be written as $\bar{V_i} = V_i e^{j\delta_i}$, $\bar{Y_{ij}} = Y_{ij}e^{j\theta_{ij}}$ and $S_{ij} = P_{ij} + jQ_{ij}$, balance equations can be derived that express P and Q as functions of δ and V. These will be referred to as the Load Flow equations:

$$P_i^{LF} = V_i \sum_{j=1}^{N} Y_{ij} V_j \cos(\delta_i - \delta_j - \theta_{ij}) \tag{2.3}$$

$$Q_i^{LF} = V_i \sum_{j=1}^{N} Y_{ij} V_j \sin(\delta_i - \delta_j - \theta_{ij}) \tag{2.4}$$

The summations in the above equations are over all N buses (the power injected at bus i must equal the sum of all line flows from that bus). On this basis, a Jacobian matrix $\mathbf{J}$ can be created:

$$\mathbf{J} = \left[\begin{array}{c|c} \frac{\partial \mathbf{P}}{\partial \boldsymbol{\delta}} & \frac{\partial \mathbf{P}}{\partial \mathbf{V}} \\ \hline \frac{\partial \mathbf{Q}}{\partial \boldsymbol{\delta}} & \frac{\partial \mathbf{Q}}{\partial \mathbf{V}} \end{array}\right] \tag{2.5}$$

The Jacobian in turn allows the creation of a linear equation system – the matrix equivalent of a first order Taylor expansion:

$$\begin{bmatrix} \Delta \mathbf{P} \\ \Delta \mathbf{Q} \end{bmatrix} = \mathbf{J} \begin{bmatrix} \Delta \boldsymbol{\delta} \\ \Delta \mathbf{V} \end{bmatrix} \tag{2.6}$$

ΔP and ΔQ are called the power mismatch equations. They express the difference between the known power injection at each bus and the injection calculated from equations (2.3) and (2.4), with an initial guess of δ and V. The very first guess is usually a "flat start" in which all voltage angles are set to zero and all voltage magnitudes to 1 p.u.[1] Equations where δ or V are already known (and P or Q are not) are omitted from the equation system. The method is iterative – $\Delta\delta$ and ΔV express the difference between the new and the old guess of δ and V. Solving the equation system for $\Delta\delta$ and ΔV allows δ and V to be updated to new, better values which will return smaller power mismatches. The process is repeated until a stop criterion is reached – usually when the power mismatches are within a defined tolerance limit [21].

The Newton-Raphson method for PF computations is applicable to all kinds of grids, both radial and meshed. However, the method involves a large set of nonlinear equations that have to be first-order Taylor approximated and solved in an iterative process. For standard PF calculations, with fixed generation and fixed configuration of the grid, this is usually a minor issue. For optimization purposes however, and especially for optimizations involving reconfiguration (R-OPF), the degrees of freedom increase exponentially and computation time becomes a major issue [2]. When tackling large systems with many degrees of freedom, it is therefore useful if other more computationally efficient methods can be found (see section 2.3.2).

2.3.2 DistFlow

In 1989, a paper was published by Mesut Baran and Felix Wu presenting a different method for solving PF and OPF problems for radial systems, known as the *DistFlow branch equations* [26]. They are a set of recursive equations, where the value at each parent bus is calculated based on the values at the forward buses (children). Consequently, they can only be applied to radial distribution systems. On the other hand, they contain only a few nonlinear terms and no trigonometric expressions. This makes them less computationally demanding, and thus more suited for optimization of large systems [2]. The DistFlow formulation of the balance equations for active and reactive power at node i are:

$$p_i^G - p_i^L = -P_i + \sum_{j \in c(i)} P_j + r_i \ell_i \tag{2.7}$$

$$q_i^G - q_i^L = -Q_i + \sum_{j \in c(i)} Q_j + x_i \ell_i \tag{2.8}$$

[1] The per-unit (p.u.) system is used in power systems analysis to normalize units across a network, thus simplifying calculations over different voltage levels. For example, the nominal voltage is always 1 p.u.

Furthermore, the DistFlow equivalents of Ohm's law and apparent power flow on a line are:

$$\nu_{\pi_i} - \nu_i = 2r_i P_i + 2x_i Q_i - (r_i^2 + x_i^2)\ell_i \tag{2.9}$$

$$\nu_{\pi_i} \ell_i = P_i^2 + Q_i^2 \tag{2.10}$$

Here ℓ_i, P_i and Q_i denote the squared line current, and the active and reactive power flow on line i, measured at the parent bus, π_i. r_i and x_i denote the series resistance and reactance of line i. p_i^L and q_i^L are the active and reactive loads at bus i, whereas p_i^G and q_i^G are the active and reactive power generation at bus i. ν_i is the square of the voltage at bus i and ν_{π_i} is the square of the voltage at the parent bus π_i. The set $c(i)$ contains all the children of bus i, namely all buses j which have i as its parent bus. If only one bus has i as a parent (i.e. if $c(i)$ only has one element), the sums in equations (2.7) and (2.8) can be written as P_{i+1} and Q_{i+1} respectively. This way the recursive nature of the equations is clearly visible. The interpretation of the power balance equations (2.7) and (2.8) is that the net power injection to a bus (generation minus load) equals the total power flowing from it towards the children of that bus, minus the power flowing towards it from the parent of that bus, with the addition of the term $r_i\ell_i$ ($P_{loss} = RI^2$) to account for the losses on the entering line (see figure 2.4). All buses except the slack bus will have one and only one entering line due to radiality, thus all losses will be accounted for.

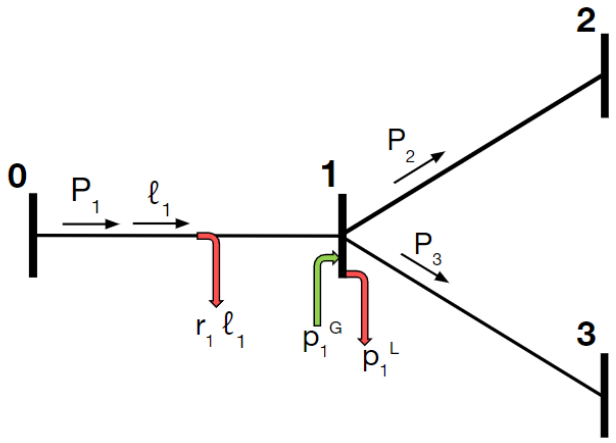

Figure 2.4: *Three-bus system showing the variables used in equation (2.7), the DistFlow active power balance equation with $i = 1$. A corresponding diagram with reactance x_1 and reactive powers Q_1, q_1^G, q_1^L could be drawn to represent the balance equation (2.8) for reactive power flow.*

In many cases the loss-term in the DistFlow equations will be significantly smaller than the power flow terms. This allows for a possible simplification of the equations by removing the loss term in equations (2.7), (2.8) and (2.9), e.g. by changing equation (2.7) to:

$$p_i^G - p_i^L \approx -P_i + \sum_{j \in c(i)} P_j \tag{2.11}$$

In addition, the constraint (2.10) is dropped entirely [2]. These new equations are referred to as the LinDistFlow equations, because all remaining constraints are linear. Linearized optimization problems allow for much faster computation. However, this simplification makes the equations less realistic and solutions less accurate according to the paper by Sou [2]. Therefore, the optimization algorithm used in this thesis is based on the more demanding but also more physically accurate DistFlow equations.

The DistFlow and Load Flow representations of PF problems are physically equivalent and both correct. For radial systems, the DistFlow equations (2.7) and (2.8) can be derived from the standard Load Flow equations (2.3) and (2.4). The practical difference between them lies in numerical solution time. The standard Load Flow formulation contains many more nonlinear terms – both equations (2.3) and (2.4) contain these terms, whereas only (2.10) of the DistFlow equation contains one. Thus for radial systems, the DistFlow equations allow for a solution algorithm that is more computationally efficient [2].

2.4 Optimal power flow

Optimal power flow (OPF) is the application of optimization to the field of PF analysis. It adds degrees of freedom to the standard PF computation by allowing some of the previously fixed quantities to vary. Instead of having an entirely fixed set of variables, including predefined generation at each bus, the OPF problem instead involves calculating some optimal steady-state value of the system, using an objective function subject to a set of constraints [27]. Some common objective functions are minimization of active power losses or maximization of some reliability index, but it can also be maximization of DG injection such as in this project.

2.4.1 Constraints

When going from fixed generation (as in PF) to variable generation (as in OPF), a set of constraints have to be introduced. These can be either equality constraints or inequality constraints. The equality constraints are generally of physical nature, such as Ohm's law and apparent power flow on a line (see DistFlow equations (2.7)-(2.10)). The inequality constraints are usually limitations on infrastructure, such as voltage and current limits for buses and lines respectively. In this thesis, the following inequality constraints are applied:

$$0 \leq \ell \leq \bar{\ell} \tag{2.12}$$

$$\underline{\nu} \leq \nu \leq \bar{\nu} \tag{2.13}$$

$$(p^G)^2 + (q^G)^2 \leq C^2 \tag{2.14}$$

$$pf \geq pf_{min} \Rightarrow |q^G| \leq \tan(\cos^{-1}(pf_{min})) \cdot p^G \tag{2.15}$$

Here $\bar{\ell}$ is the squared line current upper limit, $\underline{\nu}$ and $\bar{\nu}$ are the squared bus voltage lower and upper limit respectively, pf is the power factor (not to be confused with PF for power flow) of the generator/inverter, pf_{min} is the power factor lower limit and C is the generator/inverter apparent power rating (installed capacity). Equation (2.15) comes from the definition of the power factor (see equation (2.16)).

Equations (2.12) and (2.13) are constraints on currents and voltages in the network. These are fundamental limits that the system must operate within (see section 2.2.1). Equations (2.14) and (2.15) are constraints on active and reactive power generation. Equation (2.14) indicates, rather intuitively, that the apparent power generated can not exceed the generator/inverter apparent power rating. Equation (2.15) enforces a limit on reactive power generation based on pf_{min}. The power factor is defined as the ratio of real power and apparent power produced. It can be formulated as:

$$pf = p^G / \sqrt{(p^G)^2 + (q^G)^2} \tag{2.16}$$

In figure 2.5, the capability curve of a generator/inverter with $pf_{min} = 0.9$ can be seen:

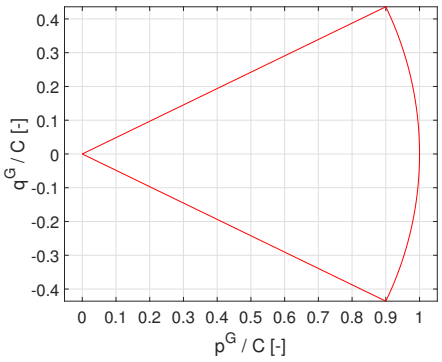

Figure 2.5: *Capability curve of a DG unit with $pf_{min} = 0.9$. Inside the red circle sector is the feasible region for active and reactive power production, p^G and q^G. The curve is scaled with the generator apparent power rating C.*

2.5 Reconfiguration

Most primary distribution systems are built in a looped or meshed structure for redundancy but are operated radially [12]. Consequently there are often lines that are not in use, referred to as *tie lines*. Lines that are connected in the normal topology are called *sectionalizing*. When opening some lines and closing others (also known as altering their *switch status*, or performing *switch events*), the topology (or *configuration*) of the system can be changed without losing its radial structure. This is referred to as *reconfiguration*.

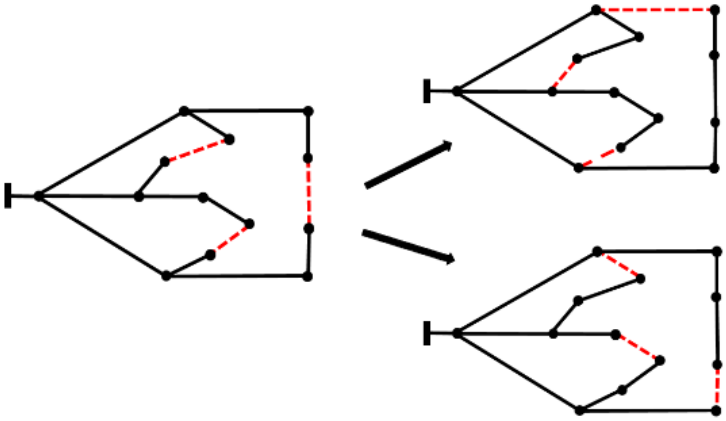

Figure 2.6: *Simple examples of reconfiguration. Red dashed lines represent disconnected lines. Note how the radial structure of the network is upheld in both cases.*

The OPF problem with fixed configuration is extended to an OPF problem with reconfiguration (R-OPF) by introducing binary switch status variables (0-1) that represent the switch status of the lines (connected/disconnected). These binary variables, π and α, are defined as:

$$\pi_{ij} = \begin{cases} 1, & \text{if bus } i \text{ is parent of } j \\ 0, & \text{otherwise} \end{cases} \tag{2.17}$$

$$\alpha_{ij} = \pi_{ij} + \pi_{ji} = \begin{cases} 1, & \text{if buses } i \text{ and } j \text{ are connected} \\ 0, & \text{otherwise} \end{cases} \tag{2.18}$$

Note that π_{ii} is always 0. With π, five terms in the DistFlow equations (2.7)-(2.10) can be reformulated as:

$$\begin{aligned} &\sum_{j\in c(i)} P_j \to \sum_{j\in\mathcal{N}} \pi_{ij} P_j \quad , \quad \sum_{j\in c(i)} Q_j \to \sum_{j\in\mathcal{N}} \pi_{ij} Q_j \\ &r_i \to \sum_{j\in\bar{\mathcal{N}}} \pi_{ji} r_{ji} \quad , \quad x_i \to \sum_{j\in\bar{\mathcal{N}}} \pi_{ji} x_{ji} \quad , \quad \nu_{\pi_i} \to \sum_{j\in\bar{\mathcal{N}}} \pi_{ij} \nu_j \end{aligned} \tag{2.19}$$

where $\mathcal{N}$ is the set of all N buses excluding the slack bus ($\mathcal{N} = \{1, ..., N\}$), and $\bar{\mathcal{N}}$ is the set of all buses including the slack bus ($\bar{\mathcal{N}} = \{0, ..., N\}$). The formulations infer that only values from active lines will come into play, and that altering the values of π alters which lines are active. This implementation is explained further in section 2.6, and visualized in figures 2.8 and 2.9.

With these formulations, all variables related to nodes such as P_i, Q_i, ν_i etc. can be written in vector form and all variables related to lines such as π_{ij}, α_{ij}, r_{ij}, etc. can be written in matrix form. For full details of these steps, we refer to the original article by Sou [2].

2.5.1 Radiality constraints

A radial network with $N+1$ buses is radial if and only if it has exactly N lines. Thus the following constraint has to be satisfied:

$$\sum_{(i,j)\in\bar{\mathcal{N}}\times\bar{\mathcal{N}}} \pi_{ij} = N \tag{2.20}$$

Having N lines however does not ensure that all nodes are connected to the network. Some might be disconnected from the network while others are connected in loops. To enforce that all nodes are connected, and thus also that no lines are connected in loops since equation (2.20) still has to be satisfied, a continuous auxiliary flow variable f is introduced:

$$\sum_{j\in\bar{\mathcal{N}}} f_{ij} - \sum_{j\in\bar{\mathcal{N}}} f_{ji} = -1, \quad i \in \mathcal{N} \tag{2.21}$$

$$0 \leq f_{ij} \leq N\pi_{ij}, \quad (i,j) \in \bar{\mathcal{N}} \times \bar{\mathcal{N}} \tag{2.22}$$

The constraints (2.21) and (2.22) ensure that one abstract unit of flow f (not power flow) can be shipped from the slack bus to each non-slack bus in the system. This is a mathematical trick to express network connectedness, not related to the physical flows in the network.

Going forward, the number of possible configurations a radially operated meshed network can have grows exponentially with the size of the network. Thus for (realistic) distribution networks with several hundreds of nodes and lines, such as in the case study of this thesis, it is too computationally demanding to search over all possible configurations. To reduce the search space of the optimization algorithm to a smaller feasible region, that returns a solution within reasonable time, the allowed number of switch events is constrained. This constraint is defined as:

$$\sum_{(i,j)\in\bar{\mathcal{N}}\times\bar{\mathcal{N}}} \left(\alpha^0_{ij}(1-\alpha_{ij}+\alpha_{ij}(1-\alpha^0_{ij})\right) \leq 2K \tag{2.23}$$

where K signifies the allowed number of switch events (starting from a predefined normal radial configuration), α^0_{ij} signifies the switch status of a line in the normal configuration and α_{ij} signifies the switch status after reconfiguration. Furthermore, for the system to remain radial and connected, all switch events must occur in pairs. No line can be disconnected without another line being connected and vice versa. Therefore reconfiguration is always run with an even number of switch events. As can be seen in chapter 3, R-OPF is most often run using $K = 0$, 2 and 4.

2.5.2 Static or dynamic

The usefulness of reconfiguration naturally depends on how often it can be performed. On the one extreme, there is static reconfiguration, where the DSO only looks for new topologies at the planning stage or at fault (yearly or seasonal time scale). This is the traditional approach and what is applied in the Eslöv network today. The other alternative is dynamic reconfiguration, where new topologies are found in real time (hourly or minute time scale) [12, 28]. Further discussion on the benefits of these approaches can be found in chapter 5.

2.6 Joint problem formulation

With the constraints defined in sections 2.3.2, 2.4.1 and 2.5.1, all essential background has been presented for the joint problem formulation of the R-OPF problem. For full details of these steps, the reader is once again referred to the original article by Sou [2]. A conceptual image of the degrees of freedom for three types of power flow computations can be seen in figure 2.7.

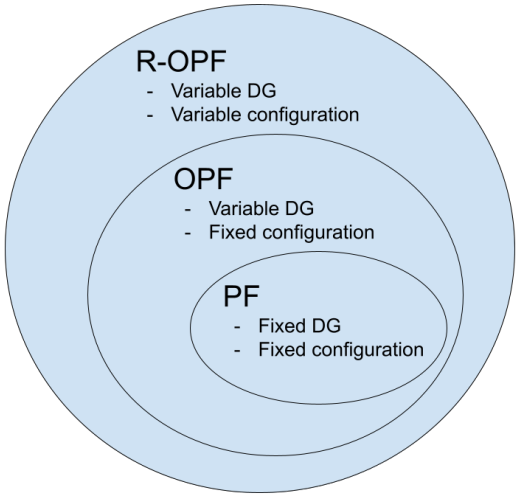

Figure 2.7: *Conceptual image of the degrees of freedom for three types of power flow computations: Reconfiguration-Optimal Power Flow (R-OPF), Optimal Power Flow (OPF) and Power Flow (PF).*

The joint R-OPF problem takes the form of a mixed-integer programming (MIP) optimization problem. It has both linear and bilinear (subset of nonlinear) constraints, but few enough of the latter to allow for a solution in reasonable time. The problem can be written on the form:

$$f(\mathbf{x}) = \frac{1}{2}\mathbf{x}^T\mathbf{Q}\mathbf{x} + \mathbf{c}^T\mathbf{x} + d$$

where $\mathbf{x}$ is the decision variable vector, $\mathbf{Q}$ defines the quadratic constraints (including bilinear) and $\mathbf{c}$ defines the linear constraints. The decision variable vector $\mathbf{x}$ is defined as:

$$\mathbf{x} = [\nu\ \nu_\pi\ \ell\ P\ Q\ p^G\ q^G\ \pi\ \alpha\ f]^T$$

and contains $7N + 1 + 3(N + 1)^2$ variables, where N is the number of nodes in the network.

The objective function of the joint problem is to maximize the input of distributed generation (i.e. the snapshot HC), and is formulated as:

$$\underset{\nu,\ell,p^G,q^G,P,Q,\pi,\alpha}{\text{maximize}} \quad \sum_{i\in\mathcal{N}} p_i^G \tag{2.24}$$

subject to the equality constrains from the DistFlow equations (2.7)-(2.10) with the reformulations in (2.19), the operational limits (2.12)-(2.15) and the radiality constraints (2.20)-(2.23).

Figures 2.8 and 2.9 below provide a visual example of the joint problem formulation. The example has four buses, four lines and one loop, so one line has to be disconnected (a tie line). The connection between $\boldsymbol{\pi}$-matrix and network topology is shown, as well as the impact of this on the DistFlow active power balance (equation (2.7)) in the joint problem formulation:

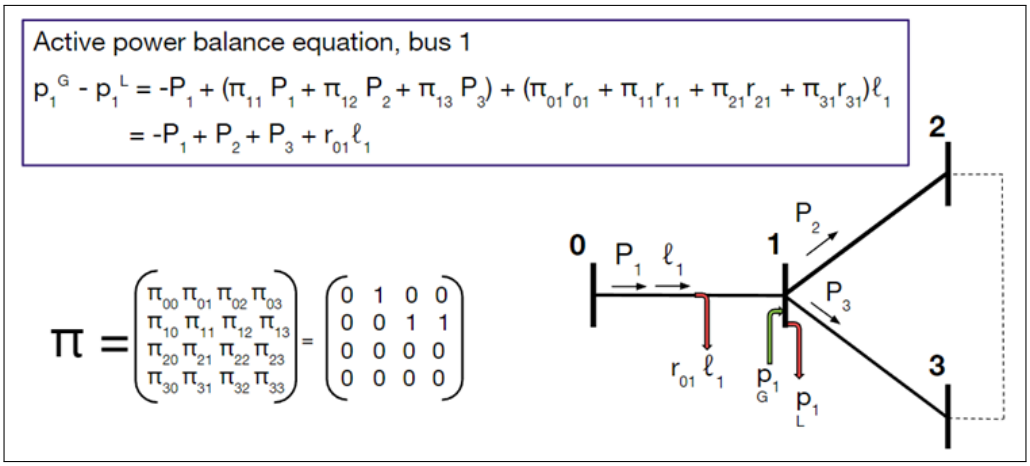

Figure 2.8: *Example of the DistFlow active power balance equation at bus 1, before reconfiguration.*

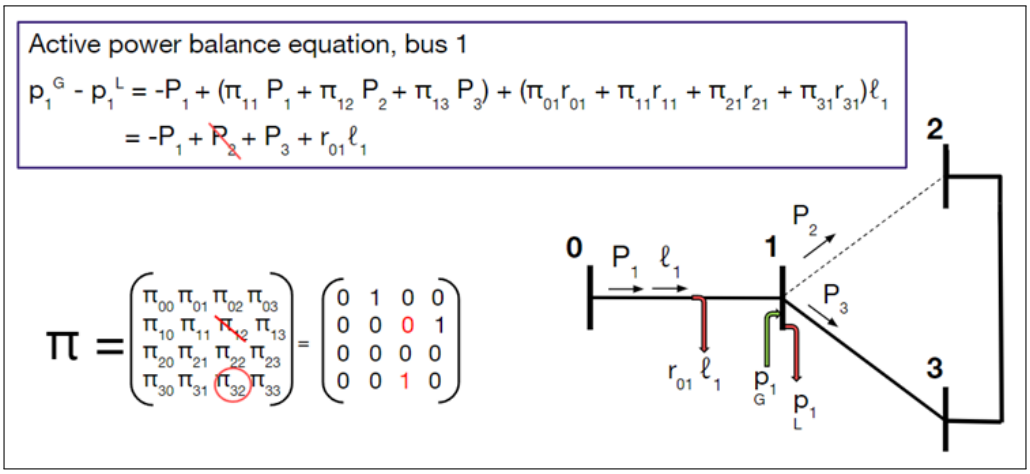

Figure 2.9: *Example of the DistFlow active power balance equation at bus 1, after reconfiguration.*

2.6.1 Solving MIPs: The branch-and-bound method

There are numerous ways of numerically solving MIP problems. The branch-and-bound algorithm is an optimization method traditionally used for linear MIP problems, but can also be extended to problems with quadratic/bilinear constraints or objectives. The method involves linear relaxation (allow discrete variables to be continuous during the solution process) and presolves the problem as if it was a linear problem. If the optimal solution is returned with a discrete variable between two integers (say, at $\pi = 0.6$), the problem is divided into two subproblems (in this case $\pi \leq 0$ and $\pi \geq 1$). It can then be shown that the optimal value of these two subproblems must be the optimal value of the problem as a whole. This "branching and bounding" is done until all discrete variables end up with integer solutions [29]. The branch-and-bound method is used in many optimization softwares, including the one used in this project (Gurobi).

Chapter 3

Method

Much of the work of this project has gone into creating an accurate model of the Eslöv distribution network, that the R-OPF algorithm described previously could then be applied to. The layout of the Eslöv distribution system will be presented in section 3.1. The chapter goes on to present how the modeling of the system was performed, in sections 3.2, 3.3 and 3.4. Finally, the simulation scenario setups that were created for running the optimization will be discussed in section 3.5.

3.1 Eslöv distribution system

The Eslöv network studied consists of a small subtransmission system with a nominal voltage of 135 kV, and a primary distribution system with a nominal voltage of 12 kV. All data concerning this system was provided by the DSO Kraftringen, which owns and operates the grid.

Eslöv S is the feed-in point from the regional subtransmission system (regionnät) operated by the DSO E.ON (130 kV), which in turn is fed from the national transmission system operated by the TSO Svenska kraftnät (400 kV). In our study, we will only look at the system operated by the DSO Kraftringen, namely what is below Eslöv S. For power flow calculations, this has the implication that Eslöv S is set as *slack bus*. The Eslöv subtransmission system in focus has three branches, connecting the transmission substation Eslöv S to the primary substations Södra Primärstationen (SP), Östra Primärstationen (ÖP) and the CHP plant Örtoftaverket (see figure 3.1). Both ÖP and SP have transformers that transform the voltage to a lower value. Together SP and ÖP make up the feed-in points to the succeeding primary distribution system.

The primary distribution system is everything at the 12 kV level, between SP + ÖP and the 468 secondary distribution stations they feed. The secondary distribution stations convert power from medium voltage (MV) to low voltage (LV) and constitute the lower scope limit of this report. All load and generation at the LV level, such as household loads and rooftop PV generations, will be aggregated at their respective secondary substation. Consequently, congestion or other issues that occur at the LV level is beyond the scope of this study.

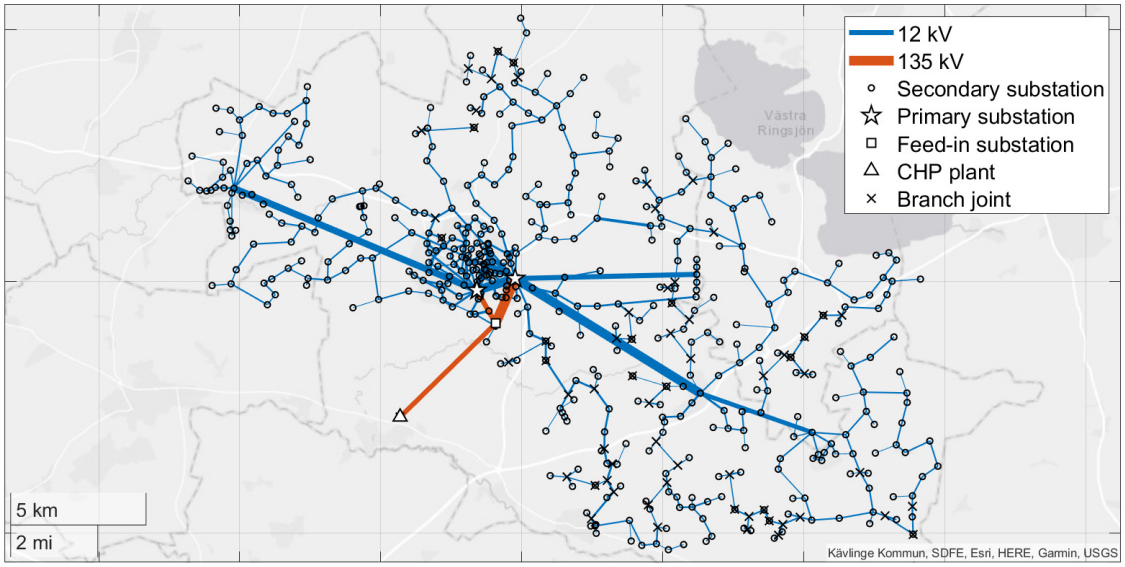

Figure 3.1: *Map of the Eslöv distribution system*[2]*, with voltage levels and substation categories. The line width is proportional to the rated current of each line.*

As can be seen in figure 3.1, there are some branches with higher current rating that feed hubs in the primary distribution system. These hubs are distribution substations (fördelningsstationer) in Marieholm (MF), Hurva (HF) and Löberöd (LF), that in turn feed a cluster of secondary substations in their respective area. Since they do not have tap-changing transformers, and operate at the same voltage as the rest of the secondary distribution system (12 kV), they are modeled in the same way as the other secondary substations in the figure above.

Table 3.1: *Specifications of the Eslöv distribution system.*

Eslöv distribution system	
Nodes	533
Feed-in substation	1
CHP plant	1
Primary substations	2
Secondary substations	468
Branch joints	61
Lines	577
Sectionalizing lines	532
Tie lines	45

3.2 Matpower modeling

The power flow model was implemented in the program Matpower. Matpower is a free, open-source extension to Matlab used to solve steady-state power system simulation and optimization problems [30]. It is widely used in research for this purpose. In this thesis, the Eslöv distribution grid is modelled as a single Matpower case. This Matpower case then constitutes the foundation for all simulations. Matpower has built in Matlab-functions for running PF and OPF simulations straight away. By adding an external optimization software, the R-OPF algorithm provided by Sou [2] can be run. In this project the *Gurobi Optimizer* software was used – a prominent solver which uses the branch-and-bound method described in section 2.6.1 [29].

[2]Most maps have a bar in the lower right corner asserting the reader that the location is Kävlinge kommun. This is not a disgraceful attempt by the authors to belittle Eslöv kommun, but an internal labeling by geoplot in Matlab.

The following data is essential input to the Matpower case:

Table 3.2: *Data required to build the Matpower case*

Input to Matpower case		
Node data: • Bus number (positive integer) • Bus type (PV, PQ, slack) • P_l, real power load [MW] • Q_l, reactive power load [MVAr] • V_{max}, maximum voltage magnitude [p.u.] • V_{min}, minimum voltage magnitude [p.u.] • S_{base}, base power of the system [MVA]	**Generator data:** • Bus number (positive integer) • P_g, real power output [MW] *only PF* • Q_g, reactive power output [MVAr] *only PF* • P_{max}, maximum real power output [MW] • Q_{max}, maximum reactive power output [MVAr] • P_{min}, minimum real power output [MW] • Q_{min}, minimum reactive power output [MVAr]	**Line data:** • From bus number (positive integer) • To bus number (positive integer) • R, resistance [p.u.] • X, reactance [p.u.] • I_{max}, rated current [p.u.] • V_{base}, base voltage [kV] • Initial branch status (1 = connected, 0 = disconnected)

In the following sections (3.3 and 3.4), the modeling of the data in table 3.2 will be described. All branch data and most of the bus data will be described in section 3.4, whereas all generator data and the bus data concerning loads will be described in section 3.5. It should be noted from start that the model is an abstraction of the actual physical system. The intention is to aggregate the physical system into a model which captures the defining characteristics of the real-world system. In figure 3.2, a summary of how the raw data was processed can be seen.

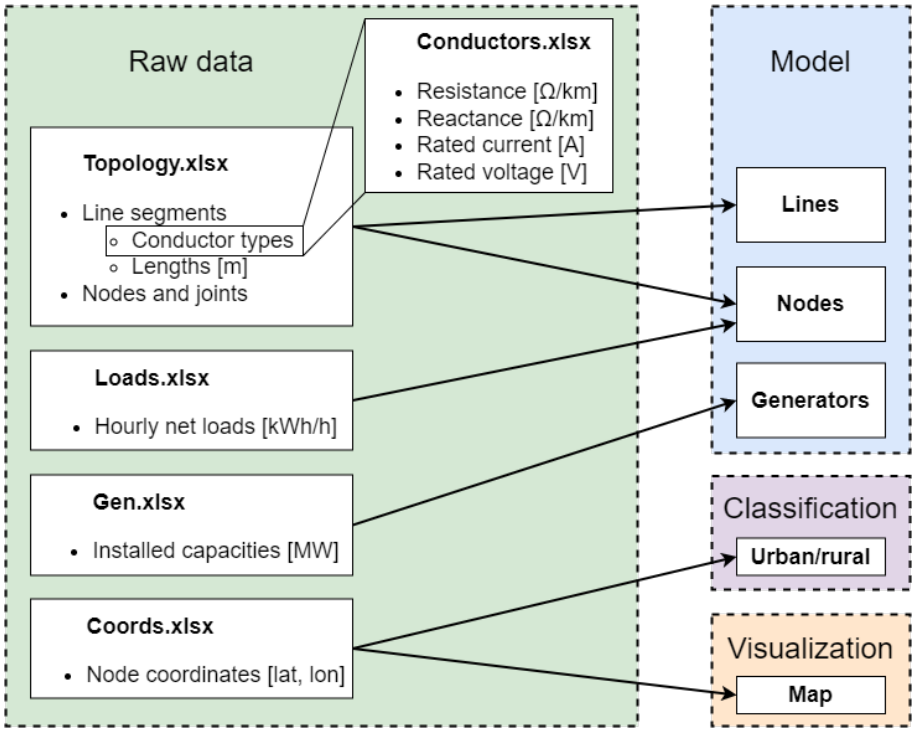

Figure 3.2: *Diagram depicting how raw data[3] was used to 1) build the Matpower case model 2) classify nodes in urban/rural and 3) visualize the system geographically.*

3.3 Modeling grid infrastructure

All networks can fundamentally be broken down into nodes and the lines connecting those nodes. Section 3.3.1 explains how the lines (or branches) are integrated into the network model, and then 3.3.2 does the same for the nodes. To conclude regarding network topology, the modeling of the normal configuration (initial branch status) is explained in section 3.3.3.

3.3.1 Branch data

Branch data for the model was extracted from Excel data sheets supplied by Kraftringen. These raw data sheets provided 1) the topology of the network and 2) specifications of all conductor types. The information extracted from the topology sheet was length, conductor type and node pair (from node ↔ to node) of each line segment. The information extracted from the conductor type specifications sheet was rated current [A], rated voltage [V], resistance and reactance per length [Ω/km] of each conductor type. Together, this constitutes all the necessary branch data for the Matpower model, except initial branch status (see table 3.2).

In the real world, there are several line segments and joints between substations, both in series and in parallel. This was also the format of the topology data sheet. To limit the size of the model, an initial challenge was therefore to aggregate line segments and joints into single lines, leaving only substations and branch joints as nodes. A branch joint is a joint where line segments divide (like a Y), in contrast to the more common straight-through joint. Straight-through joints are graphically just points on a line. They were eliminated by merging line segments in series into a single line. Branch joints connecting more than two substations are more important for the topology of the system. They were kept as nodes so that every single line could be assigned a unique node pair (see figure 3.1).

[3]The raw infrastructure data contained 1963 line segments, 73 conductor types and 622 DG units in the Eslöv system. The raw net load data contained 8760 hours x 468 secondary substations ≈ 4 100 000 values.

When merging several line segments into a single line, the equivalent impedance ($Z_{eq} = R_{eq} + jX_{eq}$) was obtained by the standard laws of combining impedances:

$$Z_{\text{eq,series}} = Z_1 + Z_2 + \cdots + Z_n$$

$$\frac{1}{Z_{\text{eq,parallel}}} = \frac{1}{Z_1} + \frac{1}{Z_2} + \cdots + \frac{1}{Z_n}$$

The equivalent rated current (I_{max}) of each single line was decided as follows: For line segments in series, the equivalent rated current was set by the line segment with the minimum rated current in the series (i.e. the bottleneck). Thereafter, the rated currents of parallel line segments were simply added up (two separate paths). For an example of how equivalent impedances and rated currents were calculated, see figure 3.3.

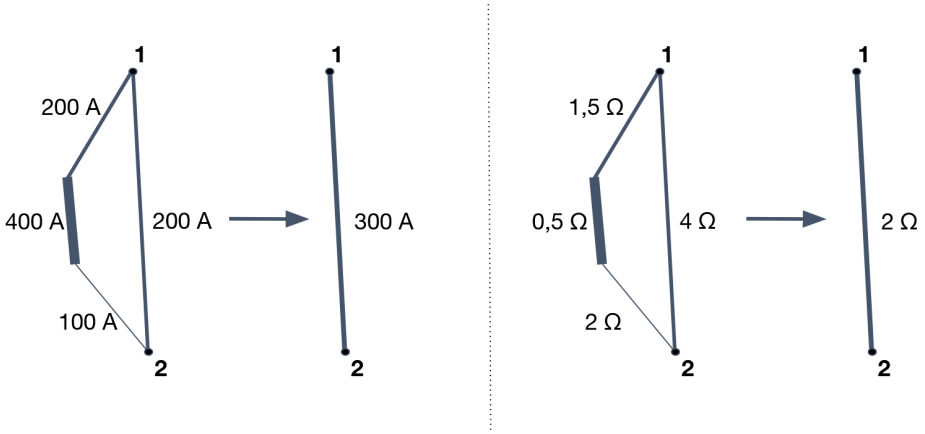

Figure 3.3: *Example of how four line segments between two nodes are merged into an equivalent single line. The left side shows how the equivalent rated current is obtained, the right side shows how the equivalent impedance is obtained.*

Some simplifications were made in the modeling of the branch data. For example, the lines were modeled as impedances with only resistance and inductance. This is a simplification that neglects for example susceptance (B) to ground. Furthermore, all secondary substations are assumed to have sectionalizing switches. The results should therefore be interpreted as where it would be beneficial to perform switch events, rather than a representation of the switching possibilities today.

It should also be noted that the Eslöv grid is a three-phase system, whereas the optimization algorithm and the Matpower case handle systems on a single-phase basis. This was managed by dividing all loads and installed generation capacities by a factor three, effectively treating each phase as a separate system. This is equivalent, since the Eslöv system is only studied in three-phase balanced steady state. After simulations were run, the actual power flows could be retrieved by simply multiplying all loads and generations with a factor three again.

3.3.2 Node data

Initially, all 533 nodes in the system were assigned a unique bus number. Eslöv S is number 1 and assigned the slack bus type. All other nodes were assigned the bus type PQ, i.e. with no voltage control. This is a slight simplification since the primary substations SP and ÖP actually have voltage control. It was deemed necessary because the optimization algorithm requires p^L and q^L at all non-slack buses to be known, and the bus voltages are calculated based on this. Since the lines Eslöv S-SP and Eslöv S-ÖP are robust and operate on a higher voltage level, ΔV over these lines is relatively small. This model choice was thus considered justifiable. Implementing voltage control in the optimization algorithm is discussed under possible improvements, see section 5.2.

Most nodes in the system are secondary distribution stations (nätstationer). In order to obtain an accurate network topology however, some nodes have been included which are simply branch joints where lines divide. These nodes exist for topology structure only, and are never connected to any loads.

After discussion with Kraftringen, and after review of similar papers on reconfiguration optimization such as the one by Sou [2], it was decided to set the minimum and maximum voltage limits to $V_{min} = 0.95$ p.u. and $V_{max} = 1.05$ p.u. at all nodes. This is also discussed in section 2.2.1 in the theory. Other papers have used $V_{max} = 1.1$ p.u. as upper voltage limit [25], thus 1.05 p.u. is a rather strict limit that should give margin to the solution regarding overvoltages.

The Matpower model was assigned an S_{base} corresponding to the rated power of the transformer in Eslöv S, namely 50 MVA. This is only used internally in the model to convert values to p.u. and should not affect the results of the optimization.

Information about the locations of the nodes was also provided by Kraftringen in the form of a coordinate Excel data sheet. Although this was not needed for the model to work per se, it greatly improved the understanding of the system and enabled visualization, such as the maps presented in this chapter. It also enabled a classification of the nodes as being either urban or rural. It was decided that all nodes within urban areas with more than 1 000 inhabitants should be classified as urban, and the remaining as rural. There are three urban areas with more than 1 000 inhabitants in the system – Eslöv, Marieholm and Löberöd. Consequently, all 112 nodes within these three urban areas were classified as urban, and the remaining 421 nodes as rural (see figure 3.4).

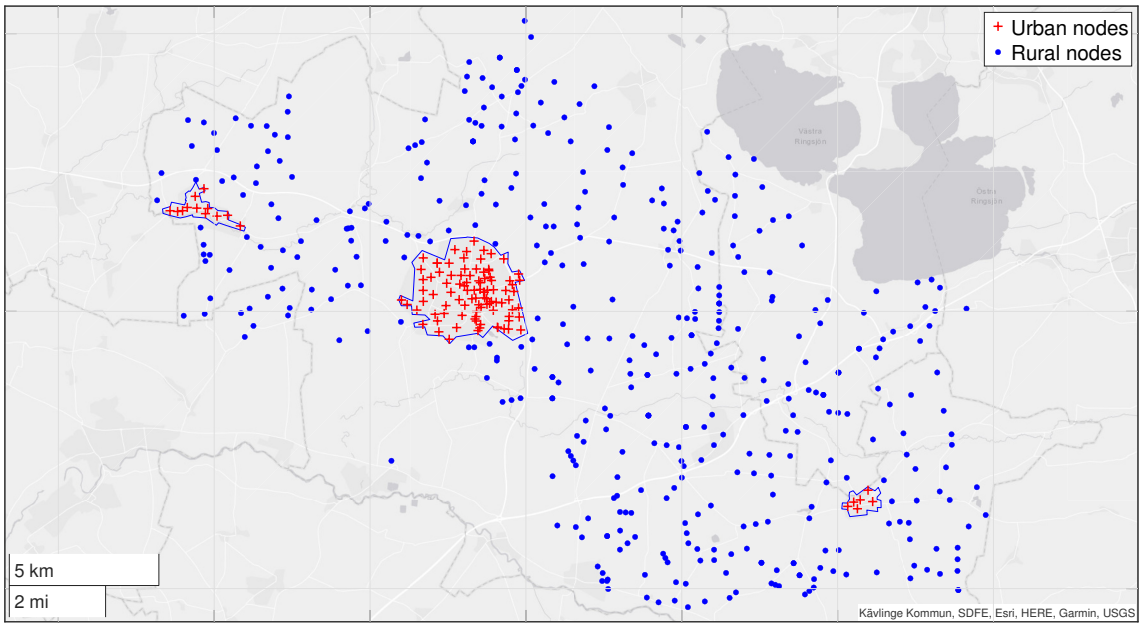

Figure 3.4: *Map showing how nodes are categorized as either urban or rural.*

3.3.3 Topology

As previously mentioned, a fundamental prerequisite for the optimization algorithm to work is that the distribution network is operated radially. This is also how the system is operated in practice. The physical system on the other hand is constructed with several loops and interconnections. Radiality thus had to be enforced by predefining a normal radial configuration.

The initial branch status of each line (1 = connected, 0 = disconnected) was determined by looking at the normal radial feeder of each node. The topology data sheet namely included a group ID of each node, which defined which radial feeder each node was normally connected to. Some nodes were assigned two group IDs, implying that these nodes could be connected to either of two radial feeders in default operation. In this case, the initial branch status that gave the best voltage profile in the system was enforced. To achieve a complete radial topology, 45 lines had to be initially disconnected, i.e. set as tie lines.

The robustness of the enforced topology was then analyzed by running a PF for the two worst-case scenarios in 2022 – the maximum and minimum net load hour. When it was confirmed that the enforced topology remained within operational limits (voltage and current) for both of these scenarios, this topology was defined as the base case for the model. Going forward, this radial topology will be referred to as the normal configuration (normalkopplingsläge), and if not explicitly stated otherwise, all R-OPF:s throughout this project will be performed using this normal configuration as starting point. This is especially important since the number of allowed switch events, K, is strictly limited, usually to no more than four switch events from the normal configuration.

In figure 3.5 a map of the normal configuration of the Eslöv system can be seen. In figure 3.6, the normal configuration of the Eslöv system can be seen as a graph, using a triangular tree layout.

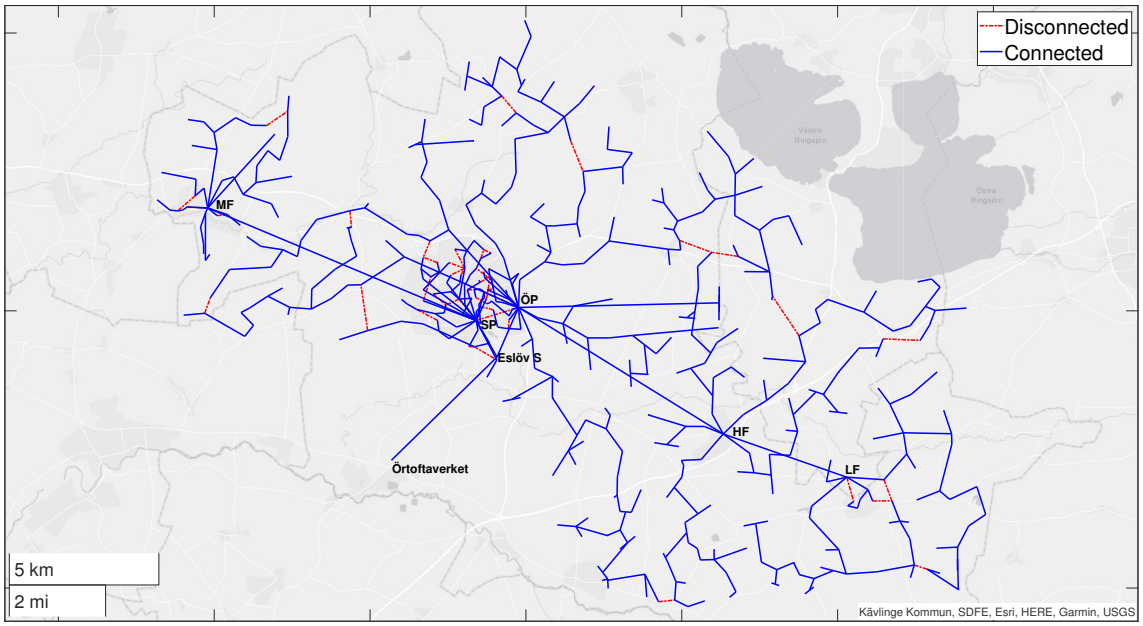

Figure 3.5: *Map of the normal configuration of the system. The blue solid lines show normally connected sectionalizing lines, whereas the red dash-dotted lines show normally disconnected tie lines.*

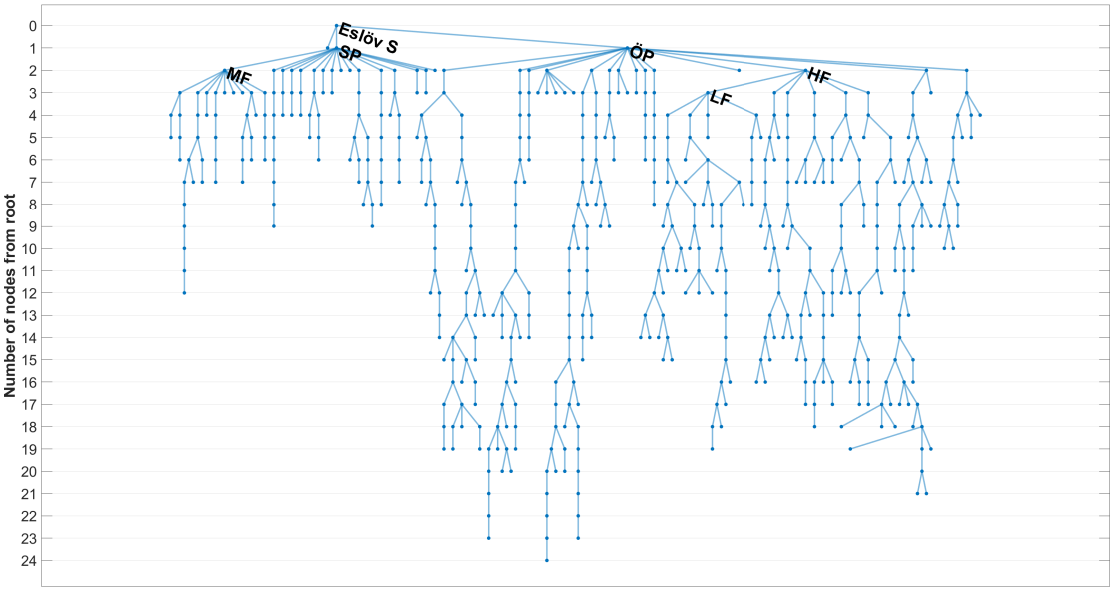

Figure 3.6: *Graph of the normal configuration of the system, using a triangular tree layout. The y-axis displays the number of nodes from the root. The longest radial feeder in the system has 24 nodes.*

3.4 Modeling generation and load

Generation data was supplied by Kraftringen in the form of an Excel data sheet providing 1) all DG units in the Eslöv distribution network 2) the nodes (secondary substations) they are connected to and 3) the installed capacity [MW] of each DG unit. In total, there are 262 nodes with DG in the network, with capacities ranging from only 3 kW up to 2 MW. The production is mostly rooftop solar PV, but in a few places wind turbines of varying sizes are also installed (see figure 3.7). The biomass-fueled CHP plant Örtoftaverket is also connected to the network (see figure 3.5). It has a capacity of 40 MW and is directly connected to the feed-in substation Eslöv S. Since it is located on a separate line connected directly to Eslöv S, it is not regarded as DG in this context. The total installed capacity in the Eslöv system, including Örtoftaverket, is 74.54 MW.

The power factor limit pf_{min} was set to 0.9 for all generators and inverters. This is an arbitrary value that is also used by Sou in [2]. In reality, the power factor of the DG units in the Eslöv network range from 0.8-1, thus 0.9 was considered a reasonable arbitrary value for existing and future DG installations. Since reactive power control is an important HC enhancement technique, the value of pf_{min} is not unimportant. However, a deeper analysis of the effects of reactive power control was decided to be out of scope for this thesis.

With the above data, the real and reactive power production limits could be defined. All DG units connected to the same node were added up to a total installed capacity, C_n. In combination with $pf_{min} = 0.9$, the feasible region for power production at each node could be defined according to the capability curve in figure 2.5.

A mismatch between the Matpower case format and the R-OPF algorithm is that Matpower only accepts rectangular shaped capability curves (with the possible addition of two sloped portions) [30], whereas the R-OPF algorithm implements a circle sector-shaped capability curve as shown in figure 2.5. The circle-sector shaped capability curve is generally a better representation of the reactive capability of wind and PV inverters [31]. This induced the decision to run OPF:s with fixed configurations using the R-OPF algorithm as well, by setting $K = 0$. The power production limits were hence not defined in the Matpower case but directly in the m-file called by Gurobi. The only built-in Matpower function used is the standard PF function, for calculation and verification when p^G and q^G are known (post-optimization or when p^G and $q^G = 0$).

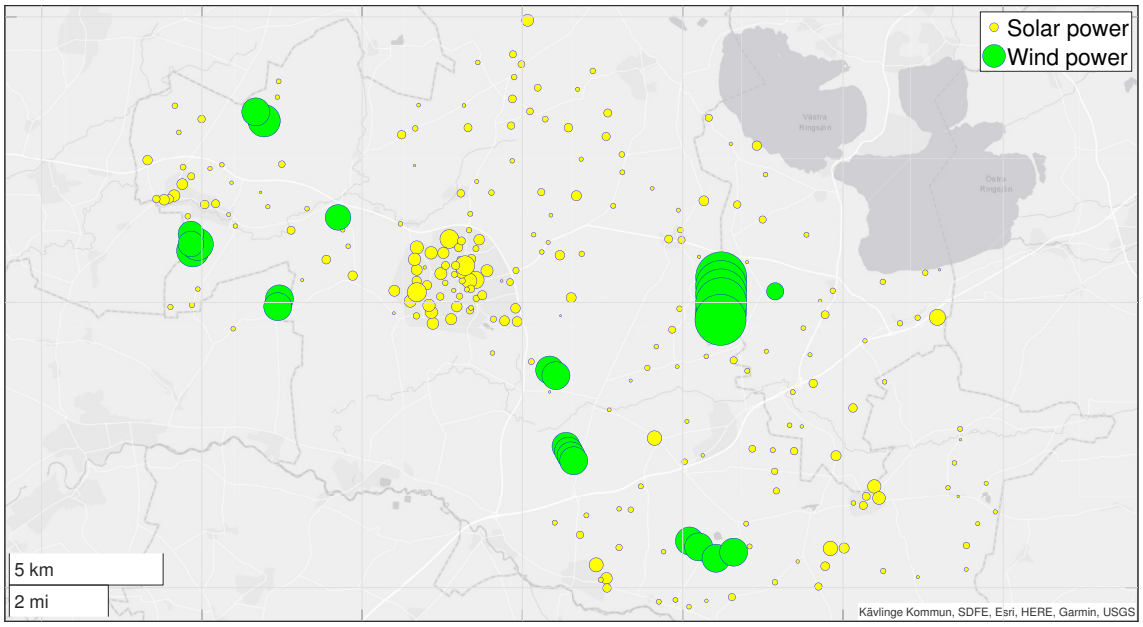

Figure 3.7: *Map showing nodes with existing DG. The area of the bubble is proportional to the installed capacity. The largest bubble corresponds to an installed capacity of 2 MW.*

Load data was also supplied by Kraftringen in the form of an Excel data sheet. This sheet provided hourly data on the real net load of each node in the system. Net load is the load minus the production ($p^L - p^G$), meaning that the load might be negative at nodes with production units installed if the generation is larger than the energy demand during a given hour. The load data was provided as average hourly values [kWh/h] for the entire year of 2022.

To model p^L for each node in the Matpower case, the load data was processed by singling out specific hours (snapshots) to work as test cases when running the R-OPF. These were the extreme cases of 2022, namely the two hours with the lowest and highest total net loads in the system respectively. The hour with the lowest total net load will be referred to as the minimum load hour and was found to be the 10^{th} of July at 14:00-15:00. The hour with the highest total net load will be referred to as the maximum load hour and was found the be the 16^{th} of December at 08:00-09:00. Of note is that during the minimum load hour (and a few other hours over the year) the total net load in the system was negative, implying that more power was produced by DG than what was consumed. At the minimum load hour, 4.25 MW was exported from the Eslöv network to the higher voltage grid, Örtoftaverket excluded. On the other hand, during the maximum load hour (and most hours annually), power had to be imported from the higher voltage grid to maintain the power balance. At the maximum load hour, 45.55 MW was imported, Örtoftaverket excluded.

The reactive loads q^L were unfortunately not included in the data sheet. Usually the reactive loads in distribution networks are small in comparison to the active loads. q^L [MVAr] was therefore arbitrarily set to $0.01 \cdot p^L$ [MW] at all nodes.

It should also be noted that the total system net load is the sum of all loads in the system. Since this is an aggregate, it does not give information about the load curve of any specific node. The minimum load hour of a single node (or even a large subset of nodes) can occur at a different point in time than the minimum load hour of the system. Consequently, there is no guarantee that the HC in a specific part of the grid is at its minimum during the minimum load hour of the system either. A really conservative approach would be to extract the minimum load hour over the year for each node individually and apply these as if they were occurring at the same time. This however would not correspond to any actual load instance, and was considered to be outside the scope of this thesis.

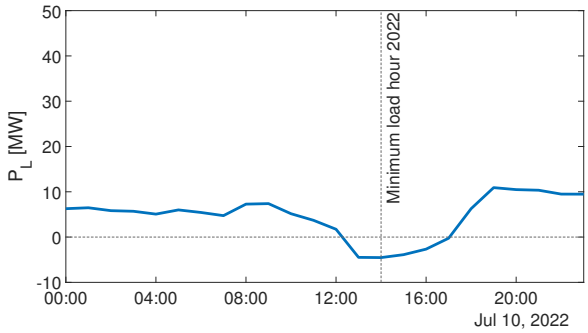

(a) Total active net load in the Eslöv distribution network on the 10^{th} of July 2022. The minimum load hour of 2022 occurred at 14:00 this day.

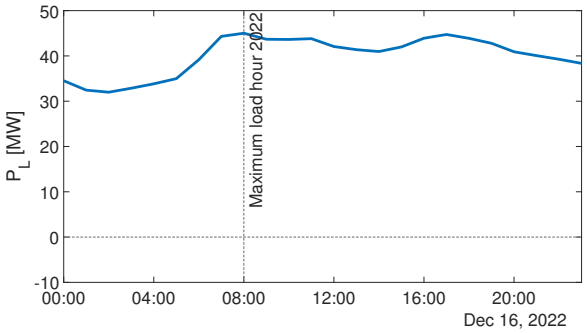

(b) Total active net load in the Eslöv distribution network on the 16^{th} of December 2022. The maximum load hour of 2022 occurred at 08:00 this day.

Figure 3.8: *Total net load in the Eslöv network for two days in 2022, Örtoftaverket excluded.*

3.5 Simulation scenario setups

One of the set research objectives for this project was to find general traits of the optimization algorithm. Another one was to quantify the increase of DG from reconfiguration in a set of defined scenarios. To answer these research objectives, a number of test cases were set up:

3.5.1 System analysis – single node generation

To gain a system overview and statistical measures of the effects of reconfigurations, tests were performed that analyzed each node in the system individually. This was then repeated for all nodes in the system. This method is often referred to as the iterative method, or the detailed method [32]. From a DSO viewpoint, this setup can be interpreted as an electricity producer wanting to connect a DG unit somewhere in the grid – in addition to already existing DG in the network.

The system analysis was structured as follows:

1. With the hourly data received from Kraftringen, apply the net load during the minimum load hour of 2022 (July 10, 14:00) to every node in the system.
2. On a single node, apply an additional large DG unit ($C = 1000$ MW). This installed capacity should be safely above any maximum generator output that the optimization can return.
3. Run the R-OPF for the three following cases:
   (a) No allowed switch events (normal configuration) ($K = 0$)
   (b) Two allowed switch events ($K = 2$)
   (c) Four allowed switch events ($K = 4$)
4. For these three cases, save the system information regarding:
   - Topology
   - Generation (HC)
   - Voltages
   - Currents
5. Repeat steps 2-4 for all 532 non-slack nodes in the system.

The purpose of adding a disproportionately large generation unit is to see when the operational limits of the grid are reached. If generation is constrained by the installed capacity of the generator (C), no information regarding the HC of the grid is retrieved. It should also be stressed that

since the hourly data provided by Kraftringen is *net* load data, existing DG in the grid is already included in the load data. Thus for this setup, all installed capacities in the generator data of the Matpower case were set to zero. Since load data is a fixed parameter, an implication of this is that existing DG was also considered a fixed parameter. An interpretation of this is that already connected DG units should not be subject to curtailment. The only generation parameter that is allowed to vary in the optimization is the active and reactive power of the single added DG unit.

Once this information was gathered, it could be analyzed in a number of ways. First and foremost, the absolute and relative increase in HC after reconfiguration was obtained. In addition, the minimum and maximum voltage in the system, as well as the maximum relative current loading in the system and the reactive power of the generator were noted, to study which operational limits were reached (active constraints). The topology was analyzed by looking at which lines were connected and disconnected.

A robustness analysis was performed for each of the cases by looking at the voltage profile in the system with the found topologies, but with the additional DG removed (p^G and $q^G = 0$). This to get a perception of if voltage limits are violated if a quick reduction in power production was to occur, such as from a fault or a sudden change in weather. It can be interpreted as a sort of N-1 criterion for the network – the system must be able to handle a dropout of the recently added DG unit.

3.5.2 Time analysis – single node generation

The test described above gives information about each node in the network, but only takes into account the behavior at a single hour of the year (the minimum load hour). It may also be of interest to see how the optimal configuration for this hour performs as the load varies over time. Ideally the effects over the entire year would be studied. However, it was determined that running that many test would take an unviable amount of time, and to some extent lead to unnecessary measurements. Instead the behavior of the system was simulated over two specific days: the days containing the minimum and the maximum load hour of the year. These will be referred to as the low-load day (10^{th} of June 2022) and the high-load day (16^{th} of December 2022). The aspiration is that by studying these two extremes, a general sense of the configuration feasibility over the year can be found. A similar technique is used and assumed valid by Capitansescu et al. in [12].

The single node chosen for this time analysis was the rural node N128, due to it being the node where the highest relative increase of HC could be seen after the system analysis. Running a simulation for a specific hour is defined as applying the net loads of this hour from the hourly load data sheet to the Matpower case. The time analysis with single node generation was structured as follows:

1. Extract the three topologies found from running R-OPF:s with DG at node N128 during the minimum load hour with $K = 0$, 2 and 4.
2. Apply these topologies as initial configurations to the Matpower case, one at a time.
3. For each of these configurations, run 24 OPF:s, one for each hour of the low-load day.
4. Save the system information for each hour regarding:
    - Topology
    - Generation (HC)
    - Voltages
    - Currents
5. Repeat the above procedure for the high-load day.

With the above method, an impression is obtained of how the HC varies over the low-load and high-load day for three static configurations. A fourth time analysis simulation was also run, this time with dynamic reconfiguration (allowing the network to perform two switch events every hour). This was structured in the following way:

1. Extract the topology found from running an R-OPF with DG at node N128 during the minimum load hour with $K = 4$.
2. Apply this topology as initial configuration to the Matpower case.
3. Run an R-OPF with $K = 2$ for the first hour of the low load day.
4. Update the initial configuration in the Matpower case to the new topology found.
5. Proceed to the next hour of the low load day and run a new R-OPF with $K = 2$.
6. Repeat steps 4-5 until the final hour of the low load day is reached.
7. Save the system information for each hour regarding:
    - Topology
    - Generation (HC)
    - Voltages
    - Currents
8. Repeat the above procedure for the high-load day.

The approach to start with the topology received from $K = 4$ and then allow 2 switch events per hour is arbitrary and can be altered with other values. From the above method, an impression is obtained of how the HC varies over the low-load and high-load day for dynamic reconfiguration, if the network is allowed to "wander away" from its normal configuration.

3.5.3 Time analysis – multiple node generation

The test above, with generation placed at only one node, makes a clear case study which is relatively easy to analyze. However, it does not make a very complete scenario of how generation might be installed in the network in the future. Nor does it make full use of the abilities of the system model and the optimization algorithm. To give some more nuance, three scenarios with DG at multiple nodes were developed and tested in the same manner as the single node generation case above. Below is a description of the three multiple node generation scenarios:

1. A scenario representing a doubling of installed generation capacity at all nodes (see figure 3.7).
2. A scenario representing expansion of wind power. Additional generation capacity of 2 MW/node was placed at 21 arbitrarily chosen rural nodes, which had no prior production (see figure 3.9).
3. A scenario representing expansion of rooftop solar. Additional generation capacity of 1 MW/node was placed at all 112 urban nodes, whether or not they had prior production (see figure 3.4).

The simulations performed on the above multiple node generation scenarios were identical to the simulations performed on the single node generation scenario, except they were only run for the low-load day (see section 3.5.2).

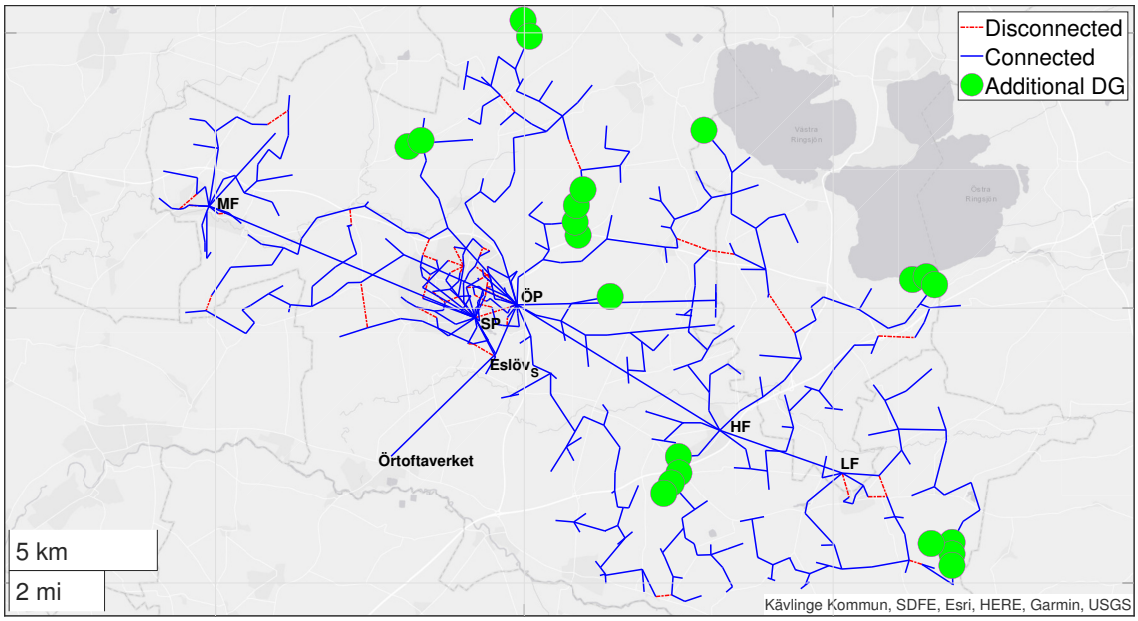

Figure 3.9: *Setup for the wind scenario in the normal configuration. Green circles show where additional DG of 2 MW/node has been placed, representing a hypothetical future expansion of wind power in the existing network.*

Chapter 4

Results and Analysis

This chapter presents the results and simultaneously a short analysis of the tests described in the method chapter. To increase the understanding of section 4.2, initially one node case is singled out and analyzed in section 4.1. The chosen node case, N128, is a rural node where the relative increase in HC turned out to be highest. Thereafter, the system analysis is presented in section 4.2, with aggregated results from all node cases. Both section 4.1 and 4.2 present results based on a single net load scenario (single point in time) and are therefore labeled as snapshot analyses. The time analysis results for the defined scenarios are presented in section 4.3. These results were obtained with varying net load, representing the hourly load data over a full day. This was done both for the single node case, N128, and for the set of scenarios listed in section 3.5.3. It should once again be stressed that the HC values refer to the additional HC, since existing DG is already included in the net load data.

4.1 Snapshot single node analysis

The node that was singled out for an initial snapshot analysis was node N128, due to it showing the largest relative increase in HC after reconfiguration (farthest to the left in figure 4.4). The intention of this approach was that it would showcase the benefits of the R-OPF most prominently. At this node, a too large DG unit was placed and R-OPF runs performed, not only with zero, two and four switch events allowed ($K = 0$, 2 and 4) as in the rest of the results, but with up to 12. For K-values higher than 12, the optimization time was deemed unacceptable and simulations were stopped. The HC at the node after each R-OPF is shown in table 4.1. The results show that the HC is strictly increasing with higher K, but that the increase is more substantial for the lower K-values, both in relative and absolute values. This indicates that the optimization, as intended, generally performs the most rewarding switch events first. The optimizations with low K-values also have smaller search spaces and thus take less time.

Table 4.1: *HC results at node N128. The table shows that both the relative and absolute gain in HC per switch event is diminishing. This shows that the algorithm, as expected, generally performs the most rewarding switch events first. The optimization time increases with the number of allowed switch events.*

Number of allowed switch events (K)	0	2	4	6	8	10	12
Hosting capacity [MW]	1.14	2.69	3.57	4.14	5.01	5.38	5.39
Relative incr. from prev. column [%]	-	135%	33%	16%	21%	7%	0%
Absolute incr. from prev. column [MW]	-	1.55	0.88	0.57	0.87	0.37	0.01
Optimization time[4] **[s]**	2	71	81	293	619	1261	3098

[4]Run on a computer with 6 core processor and 3.79 GHz clock rate.

Figure 4.1 contains the same information as table 4.1 about the absolute increase in HC, but with only $K = 0$, 2 and 4. The figure displays the HC as a 3D bar chart, with the height (z-direction) representing the HC [MW] and the x,y-coordinates representing the location of the node in the grid. Figure 4.3 in section 4.2 is a systemwide extension of this figure.

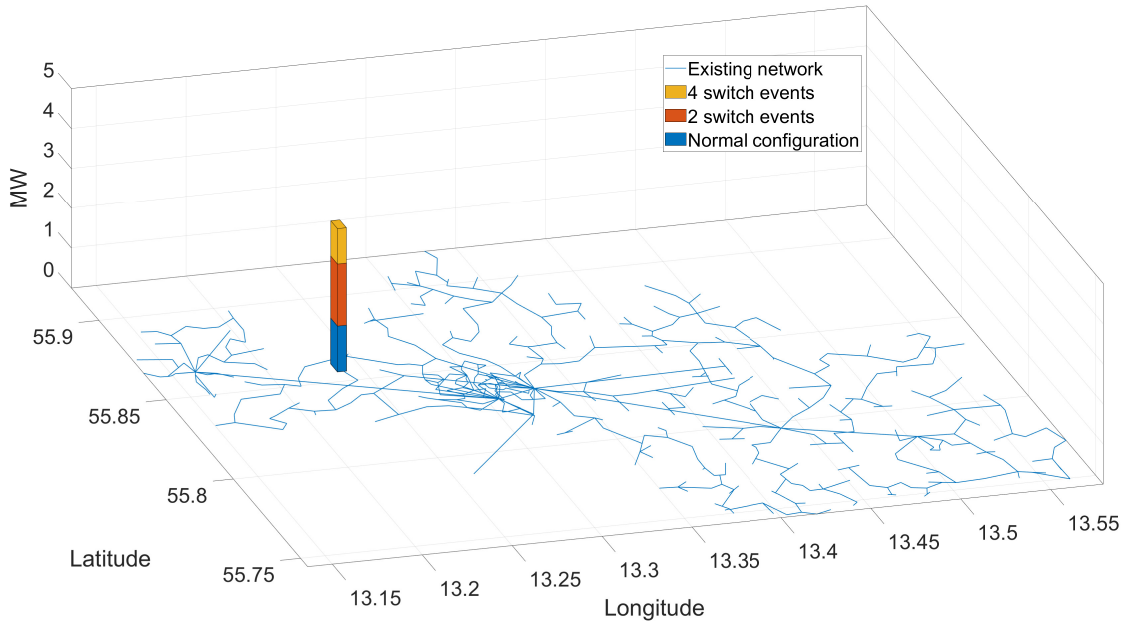

Figure 4.1: *3D bar chart displaying the HC at node N128 during the minimum load hour of 2022. The height (z-value) represents the HC [MW] and the x,y-coordinates represent the location of node N128 in the grid. The HC is shown both for the normal configuration ($K = 0$) and for the new configurations after two and four switch events ($K = 2$ and 4), in accordance with the values in table 4.1.*

In figure 4.2, the topology of the grid is shown for the three above-mentioned scenarios ($K = 0$, 2 and 4), with the map zoomed in around the location of N128. In the reconfiguration between subfigures 4.2a and 4.2b, two switch events have been performed which alter the radial feeder that N128 is connected to (switching from its northern to southern feeder). In subfigure 4.2c, four switch events have been performed (although only two are visible in the zoomed-in frame). N128 is now connected to both its northern and southern feeder, almost forming a loop, but a disconnection has occurred on a line connected to the primary substation ÖP (see bottom-right corner of subfigure).

Node N128 is now located on a longer radial than before, with more nodes from root to leaf. This phenomenon, that the algorithm returns topologies where the DG unit(s) end up on long radials, has been observed in several scenarios throughout the project and is a general trait of the algorithm. An explanation to why this occurs is that high active loads weigh down the voltage when there is a considerable resistive component in the lines (see equation 2.1). This is the case for most rural distribution networks. Thus when there is more active load on the radial, the voltage decreases and higher amounts of DG can be injected before the upper voltage limit is reached.

In the top left corner of the subfigures in figure 4.2, a number of other key values of the system are shown. These are 1) the HC at node N128, 2) the minimum and maximum node voltage (v_{min} and v_{max}) in the system and 3) the maximum line loading $|I|/|I_{rated}|$ in the system. The upper voltage limit is hit in all cases, making it an active constraint for more HC in all cases. In 4.2b and 4.2c the upper current limit is hit as well, making it another active constraint for more HC. This development is reasonable, as the optimization algorithm strives to use the network to its full capacity, thus bringing the operation towards additional operational limits.

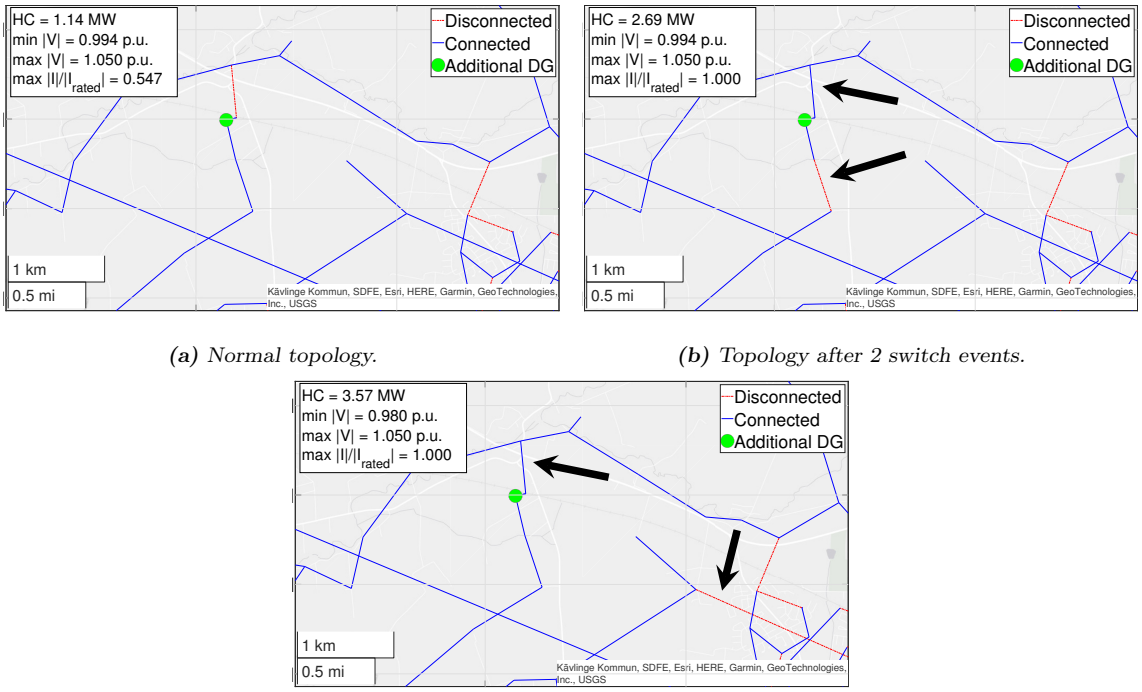

(a) *Normal topology.*

(b) *Topology after 2 switch events.*

(c) *Topology after 4 switch events.*

Figure 4.2: *Maps zoomed in around node N128 to show the normal configuration and the changes in topology after switch events are performed. The figures show the HC at node N128 (corresponding to the values in table 4.1), the minimum and maximum voltage (v_{min} and v_{max}) in the network, and the maximum line loading ($|I|/|I_{rated}|$) in the network. In (a) only the voltage limit is reached (the voltage is 1.05 p.u. somewhere in the system), but in (b) and (c) both voltage and current limits are reached. Between (a) and (b), the radial feeder that N128 is connected to has switched from its northern to southern feeder. In (c), N128 has been connected to both its northern and southern feeder, almost forming a loop, but a disconnection has occurred on a line connected to ÖP (see bottom-right corner of subfigure). The other pair of switch events (not visible in frame) resulted in the disconnection of a line connected to SP.*

4.2 Snapshot system analysis

The same results that were generated for node N128 can also be generated for all other 531 non-slack nodes in the system. This section presents the aggregate results of those simulations. This will be referred to as the system analysis. When performing the simulations for the system analysis, only simulations with zero, two and four switch events were considered ($K = 0$, 2 and 4), due to the long optimization time for R-OPF:s with higher K-values.

4.2.1 Hosting capacity improvement

The same information as in figure 4.1 can be presented for all nodes in the system simultaneously. This is done in figure 4.3. Each bar represents three optimizations ($K = 0$, 2 and 4), with DG placed *only* at the node where the bar is located. The results from the nodes SP, ÖP, Eslöv S and Örtoftaverket (see figure 3.1) have been removed from the figure, since the HC at these nodes is much larger than in the rest of the system, and because generation at these nodes can hardly be called distributed. The figure shows that the HC varies widely with the location in the network. Looking at the bar heights, we see that the HC ranges from only a few up to 30 MW, with the HC in general being higher within the Eslöv urban area. There are some notable exceptions, for example the distribution substations LF and HF that can be seen as tall bars in the southeastern part of the network. Some bars are almost completely blue, indicating that reconfiguration caused no significant increase in HC at these locations. Other nodes have had their HC more than doubled by reconfiguration, either after two switch events or after four. In some cases, the results vary greatly

even between neighbouring nodes. This might be due to them being electrically separated in the normal configuration, but could also have other causes. Apparently, the results from a single node case, such as the ones from N128 above, reveal very little about the system as a whole. All single node cases must be analyzed as a collective. This is done in the remaining part of this section, and in chapter 5.

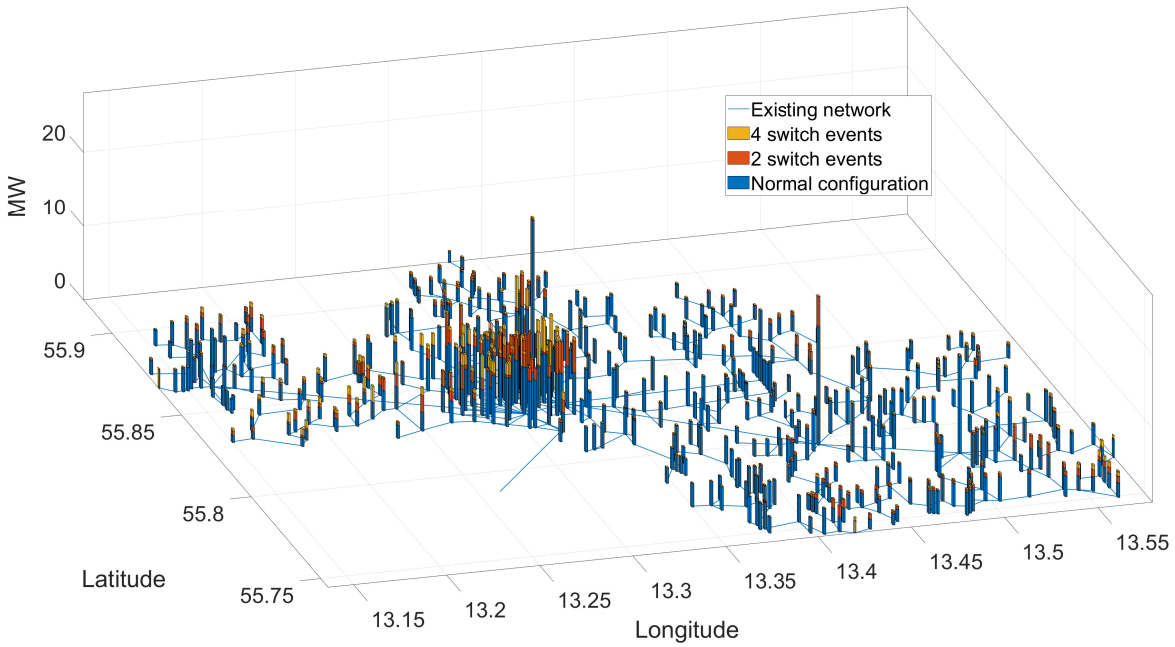

Figure 4.3: *3D bar chart displaying the HC at all distributed nodes in the network during the minimum load hour in 2022. The height (z-value) represents the HC [MW] and the x,y-coordinates represent the location of the node. The HC is shown both for the normal configuration ($K = 0$) and for the new configurations after two and four switch events ($K = 2$ and 4). Note that each bar represents an R-OPF run with DG only at a single site (at the indicated point), not that DG has been placed at all nodes simultaneously. A large range of results can be seen, both in terms of absolute HC values and the relative increase from reconfiguration. As an example, the entirely blue bars are at nodes where reconfiguration had no effect on the HC.*

To get a general sense of the benefits of reconfiguration, figure 4.4 was produced. In this, the relative increase in HC for all node cases can be seen, sorted in descending order of magnitude. The figure can be interpreted as how many percent of the node cases, x %, exhibit a relative increase in HC of y % or higher from reconfiguration. As expected, the relative increase is higher for $K = 4$ than for $K = 2$. Note that both the red and the yellow bars are sorted in descending order, implying that two bars at the same x-value must not correspond to the same node case. The figure once again illustrates the large spread of the results. In about 9% of the node cases, the HC can be improved with more than 50% through reconfiguration with $K = 2$. If $K = 4$, about 16% of the node cases show a relative increase of more than 50%. In contrast, around 30% of the node cases show a relative HC increase of less than 5%, even after reconfiguration with $K = 4$. The mean HC increase for all node cases with $K = 4$ is 23.9%, but the median is only 10.6%. This difference implies (as can also be seen in the figure) that the data is not very evenly distributed, and has large outliers. Simply put, the effect of reconfiguration is very much dependent on where DG is connected.

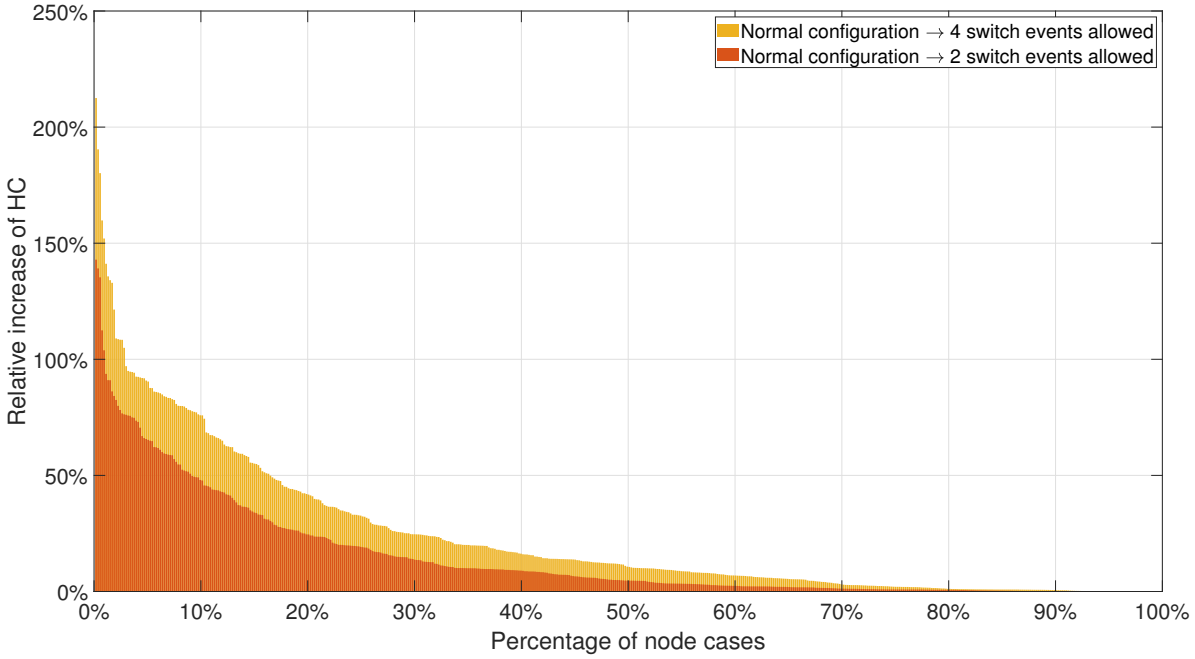

Figure 4.4: *The relative increase in HC after reconfiguration for all node cases, sorted in descending order of magnitude. The figure can be interpreted as how many percent of the node cases, x%, exhibit a relative HC increase of y% or higher from reconfiguration. The highest relative increase in HC for $K = 2$ is 142% and for $K = 4$ it is 212%. The mean increase for all node cases with $K = 4$ is 23.9%, but the median is only 10.6%. About 30% of the node cases show no significant increase (¡ 5%) in HC from reconfiguration.*

After examination of figure 4.3, it was decided that the difference between urban and rural nodes required further study. A result of this can be seen in figure 4.5, where the data in figure 4.4 has been divided into urban and rural data sets and subfigures. There is a clear difference between the distributions. Among the rural node cases, the largest relative increases for individual node cases can be found, but the majority of the rural cases exhibit a rather small relative increase from reconfiguration. Among the urban nodes cases, the largest relative increases for individual node cases are smaller but there is a significant relative increase for a higher number of cases, especially after four switch events. Only about 12% of the rural nodes have their HC increased with more than 50% after R-OPF with $K = 4$, whereas that number for urban nodes is 24%. The results suggest that for nodes further out in the system (rural), the HC can sometimes be greatly improved through reconfiguration if the normal topology is not favourable. This is for example the case with N128 mentioned before. In many cases however, there is not much to do in terms of reconfiguration, due to there being a lack of switch options in rural areas where the network topology is more radial. In the urban areas, the grid is more densely looped or meshed, which gives rise to more possibilities for reconfiguration.

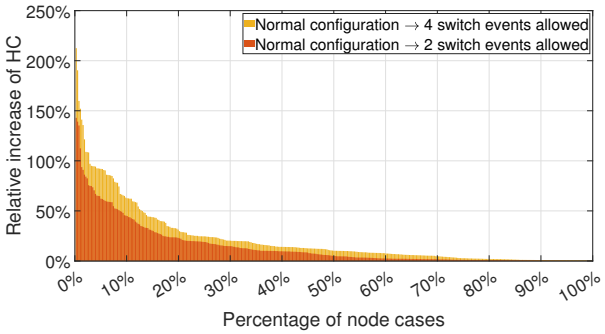

(a) Relative HC increase in ***rural nodes****. The figure can be interpreted as how many percent of the rural node cases, $x\%$, exhibit a relative HC increase of $y\%$ or higher from reconfiguration.*

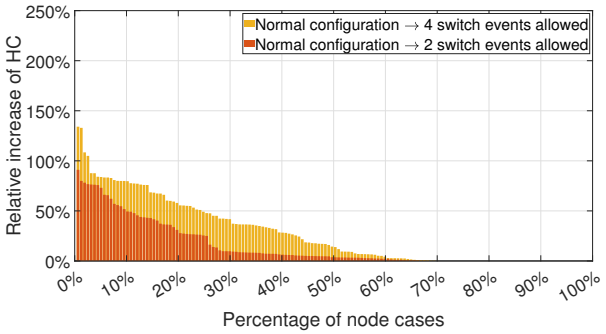

(b) Relative HC increase in ***urban nodes****. The figure can be interpreted as how many percent of the urban node cases, $x\%$, exhibit a relative HC increase of $y\%$ or higher from reconfiguration.*

Figure 4.5: *The relative increase of HC after reconfiguration, with nodes separated in the classifications rural and urban. In rural areas, the benefit of reconfiguration is more varied. The largest relative increases for individual node cases are found in the rural areas, whereas twice as many node cases in the urban areas show a relative HC increase of 50% or more from reconfiguration with $K = 4$.*

4.2.2 Active constraints

When analyzing the maximum HC at different nodes, it is of course of interest to know which factors are limiting. In optimization terms, these limiting factors are called active constraints. The two most fundamental operational limits of the network, and the ones considered in this report, are the voltage and current (thermal) limits. Another potentially limiting factor, that is not an operational limit of the network in itself but is strongly related to the node voltages, is the power factor, pf. If pf is at 0.9, the reactive power produced or consumed by the generator/inverter is maximized. In this project, the challenge is most often to avoid overvoltages close to the DG unit, thus reactive power is mainly consumed by the generator/inverter.

Figure 4.6 shows in how many node cases the above mentioned factors are limiting (active constraints), as a percentage of all node cases. The voltage limit in this context is always the upper voltage limit (1.05 p.u.), since this is the one hindering further DG injection. The results are categorized in urban/rural and in $K = 0$, 2 and 4 allowed switch events. A constraint is considered active if 1) $|V| = 1.05$ p.u. 2) $|I|/|I_{rated}| = 1$ and 3) $pf = 0.9$ at any node in the system respectively. Note that more than one constraint can be active in each case.

In general, it can be seen that both voltage and current constraints are active more frequently after reconfiguration has been performed. This, as mentioned before, can be interpreted as the algorithm trying to utilize the grid to its full capacity, thereby finding topologies where the system can operate closer to more of its operational limits. A notable exception to this is the current constraint in urban areas, which is active less frequently after reconfiguration. Since the current constraint is active in almost 100% of the urban cases already with $K = 0$, there is not much room for increasing this share further, but why the share is decreasing is hard to explain. It might have to do with the voltage limit coming into play more often after reconfiguration, thus reaching this limit instead of the current limit but this is mere speculation and contradicts the previous statement regarding several limits reached simultaneously.

The voltage constraint comes into play more often in rural node cases than in urban, which is expected since the rural grid has longer radials extending far from the voltage-controlled slack-bus, resulting in larger voltage variations. For the opposite reason, the current limit is active more often in the urban node cases. Similar results can be found in the thesis by T. Walla [25], who when researching the HC in Swedish distribution grids found that current was a more limiting factor than voltage in urban grids, and vice versa in rural grids.

The power factor constraint is another interesting result. Apparently, pf is less frequently a limiting factor in rural areas after reconfiguration has been performed, and in urban areas it is almost never an active constraint. The pf limit is closely correlated with the voltage limit, since the pf limit controls reactive power input/output which in turn controls the bus voltage. It was observed in the beginning of this project that the R-OPF algorithm often returns long radials with both low and high node voltages along the DG radial, in contrast to the normal configuration where the node voltages along the DG radial were often just high. If the generator/inverter has to balance both high and low voltages along a radial, the reactive power output of the DG unit is likely to be somewhere in between its operational limits, and the pf constraint would then not be active. An example of this can be seen in the 33-bus example in Sou's paper: with $K = 0$, the minimum pf is 0.9 (active constraint) but with $K = 4$, the minimum pf is 0.97 (inactive) [2].

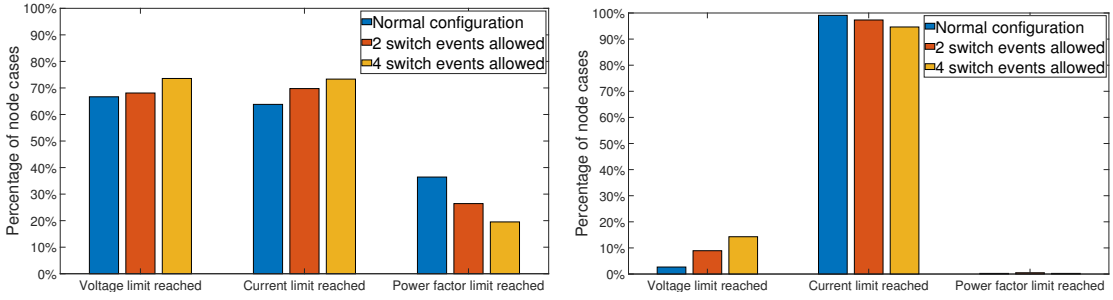

(a) *Active constraints in* ***rural*** *node cases.*

(b) *Active constraints in* ***urban*** *node cases.*

Figure 4.6: *Bar charts displaying in how many node cases the voltage, current and power factor limit is reached, as a percentage of all node cases in the respective category. The voltage limit is considered reached if $|V| = 1.05$ p.u. at any node in the system, the current limit if $|I|/|I_{rated}| = 1$ at any line in the system, and the power factor limit if $pf = 0.9$ at the (single) DG unit. Results are classified in urban/rural and in $K = 0$, 2 and 4 allowed switch events. Note that more than one constraint can be active in each case. In general, voltage and current constraints are active more often after reconfiguration, indicating that the system takes advantage of more of its operational limits with the new topologies. As expected, voltage is more often the limiting factor in rural areas than in urban.*

4.2.3 Robustness analysis

When performing reconfigurations based on a specific load scenario, it is important to consider the robustness of the newly found topologies if the load scenario was to change. Performing reconfigurations based on the minimum load hour is in one way adequate, since this is the hour most limiting to the HC. If the grid can accept a given amount of MW at the minimum load hour, it can likely accept the same amount at another time of the year, when overvoltages are less likely and local demand can absorb more of the DG. On the other hand, the minimum load hour is a very extreme case that is not representative of the rest of the year, since the load stress of the system is then at its lowest. A robustness analysis is needed to judge the new configurations, e.g. if DG was to suddenly drop (due to a fault or a sudden change in weather), or if the load was to increase. A sudden lapse of a DG unit can be seen as testing the N-1 criterion for that unit.

In the system analysis, new HC maximizing topologies were found for every single node case. Figure 4.2 is only one of 532 examples of how the topology can change. With all newly found configurations (both with $K = 2$ and 4), PF simulations were run with new predefined load scenarios. The first choice, that was defined for all PF simulations, was to have DG removed ($p^G = 0$), instead of at its maximum HC (that the R-OPF otherwise returns by default). The second choice was to run PF simulations both during the minimum and maximum load hour of the year. For all these 2 x 2 x 532 simulations, the minimum voltage in the system, v_{min}, was saved. The results can be seen in figure 4.7. The minimum voltage for each of the cases is presented in three levels. The first level is where v_{min} remained within its design limits (> 0.95 p.u.). The second level is where v_{min} dropped below its design limits, but is still above acceptable operational limits (> 0.9 p.u.). The third case is where v_{min} dropped below 0.9 p.u.

If only p^G vanishes, but the minimum load hour scenario remains, figure 4.7 shows that the configurations hold up the voltage profile well in almost all cases. This is especially the case if only two switch events were allowed in the reconfiguration. In contrast, if the load increases drastically to the maximum load hour scenario, at the same time as p^G drops, the voltage drops below 0.95 p.u. in the majority of cases. If four switch events have been allowed, v_{min} even drops below 0.9 p.u. in the majority of cases.

Some of the cases simulated here are of course extreme. It is not very likely that all DG production disappears at the same time as the power demand suddenly increases to yearly peak levels. At the same time, it is a scenario worth considering, since it illustrates a risk that could come into play in milder scenarios as well. For future work, finding new configurations based on the maximum load hour of the year is worth considering as well, as these will be more inherently robust (R-OPF based on high load stress in the grid). On the downside, optimizing based on the maximum load hour will likely give a too generous estimate of the HC.

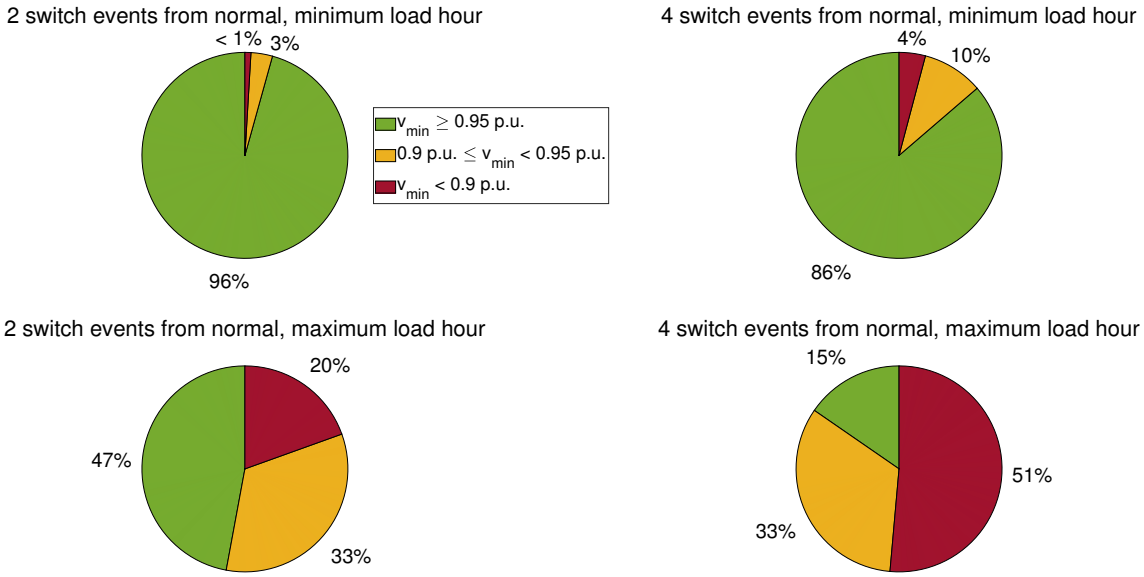

Figure 4.7: *Pie charts of the minimum voltage in the system (v_{min}) if production vanishes. For each node case, DG was placed at a single node and an R-OPF was performed based on the minimum load hour. The production at the single node was then removed and a PF simulation was run using the newly found network topologies. The two top charts show which voltage interval v_{min} ends up in if production at the single node drops, from maximum HC to zero, but the minimum load hour scenario remains. The two bottom charts show which voltage interval v_{min} ends up in if production at the single node drops, and the loads in addition change drastically, to the maximum load hour scenario. The results show that with more switch events allowed ($K = 4$), more of the newly found configurations are likely to show a large drop in voltage if production falls away, than if fewer switch events were allowed ($K = 2$) when the new configurations were found. Moreover, the results show that a large part of the newly found configurations can not be implemented as new, static configurations straight away.*

4.3 Time analysis

The results in figure 4.7 provide information about how the system will behave after reconfiguration if conditions are altered. Looking further into this, the tests described in sections 3.5.2 and 3.5.3 were performed, to find the HC over a whole day rather than just at a snapshot in time. This is a first step towards analyzing how much more energy [MWh] the grid can accept through reconfiguration, rather than just power [MW] at a single point in time. In addition to the HC, the minimum voltage in the system will be presented over the day, as this gives a hint regarding how robust each new configuration is. For one case (the N128 single node case), HC results are presented for the day with the maximum load hour as well. In section 4.3.1, the single node analysis from section 4.1 will be expanded on. Sections 4.3.2-4.3.4 will then present the multiple node generation scenarios – the double generation scenario, the wind scenario and the solar scenario.

4.3.1 Single node – N128

The blue, red and yellow curve in figure 4.8 shows the HC at node N128 using the three static configurations found with $K = 0$, 2 and 4 allowed switch events respectively. These configurations are held constant over the day while the load is varied. Note that the values of the bar in figure 4.1, which shows the snapshot HC of the three configurations, actually equals the values of the blue, red and yellow curve in figure 4.8 at the minimum load hour (dashed line at 14:00). In addition, the purple curve shows a dynamic reconfiguration simulation, where the topology has started with the $K = 4$ topology and then been allowed to reconfigure with two switch events every hour (including the first hour).

The results show that the increase in HC that was seen at the minimum load hour is maintained over the day, indicating that the new configurations are helpful in other load scenarios than the minimum one. There is, as expected, energy to be gained over time through reconfiguration. For example, with the $K = 2$ configuration, an additional 1-2 MW can be injected throughout the day, resulting in an energy gain of about 30 MWh. The HC is at its minimum, or close to its minimum, during the minimum load hour, which justifies the choice to base simulations on the minimum load hour. The dynamic reconfiguration performs better than the $K = 4$ static configuration, which is also expected since the R-OPF in dynamic mode is allowed to perform more switch events throughout the day, hence wandering away from the normal configuration and fine-tuning the topology of the grid continuously. However, it displays a more variable and irregular behavior due to the switching. At the minimum load hour, the dynamic reconfiguration returns a configuration where the HC can be increased significantly, but this configuration is only feasible during this extreme low load scenario. At the adjacent hours, the HC drops back to values closer to the $K = 4$ curve again.

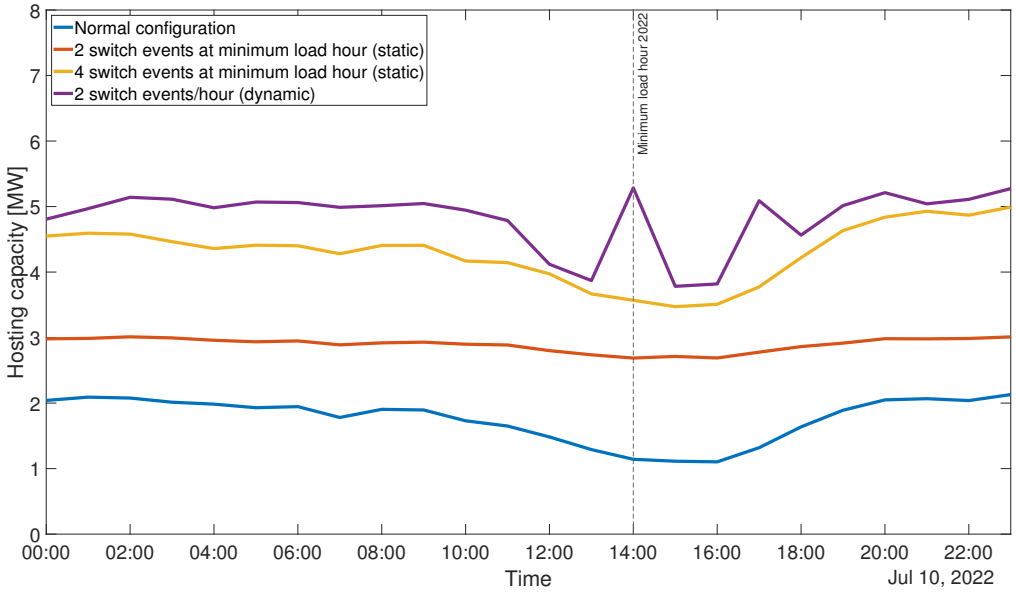

Figure 4.8: *Graph of the amount of generation that the grid can accept (snapshot HC) at node N128 during the* ***minimum*** *load day. Simulations are based on net load data, thus the y-values can be interpreted as the additional DG that can be injected at the node. The blue, red and yellow curves are static configurations, found from R-OPF:s based on the minimum load hour. The purple curve represents dynamic reconfiguration, with two switch events allowed per hour. The increase in HC that was found at the minimum load hour is present throughout the whole day, thus there is energy to be gained from reconfiguration. Dynamic reconfiguration gives larger improvement than static, but also demonstrates a more erratic behavior. The HC is at, or close to, its minimum at the minimum load hour.*

To gain additional understanding of the system after reconfiguration, it was decided to also study the voltage profile in the system over the day. However, studying all bus voltages in the system for all hours of the day and all configurations would be too extensive, thus it was decided to focus only on the minimum voltage in the system (v_{min}) for each time and configuration. Note that v_{min} does not have to occur at the same node throughout the day, but can change location as the load scenario fluctuates (and in the dynamic case, as the configurations change). This explains the sometimes large variations in the v_{min} curves.

There are two main reasons for studying v_{min} in depth. First, v_{min} gives a hint about the robustness of a new configuration. If v_{min} is low, the configuration is less likely to sustain a good voltage profile in case of a load or generation change. Second, it is of interest to analyze the spread of bus voltages across the system. It is generally desirable to keep voltage deviations small, close to the nominal voltage across the whole system. If all bus voltages are high for example, it is easier to lower the voltage using e.g. a tap-changing transformer. If there are both high and low voltages on the other hand, there is less room for action. Thus it is of interest to keep v_{min} high, close to the nominal 1 p.u. Analyzing the maximum voltage (v_{max}) or current loading in the system in depth was considered superfluous, since these are often at their operational limit, or expected to be at their limit (maxed out, at 1.05 p.u. and 1 respectively).

Looking at figure 4.9, we see that v_{min} is close to 0.99 p.u. for both the normal configuration and the $K = 2$ configuration throughout the day. With the $K = 4$ configuration and the dynamic configurations however, v_{min} exhibits a drop towards the lower voltage limit. Especially with dynamic reconfiguration, v_{min} is often really close to the lower 0.95 p.u. limit, as the R-OPF algorithm continuously fine-tunes the topologies and constructs long radials that weigh down the bus voltages along the DG radial as much as possible. Having these lower minimum system voltages is a disadvantage of the $K = 4$ configuration and dynamic reconfiguration. One can also see an inverse behaviour between the HC dynamic (purple) curve in figure 4.8 and the v_{min} dynamic (purple) curve in figure 4.9. When v_{min} is close to 0.95 p.u. during dynamic reconfiguration, such as at the minimum load hour, the increase in HC is more dramatic. During the adjacent hours, this HC-beneficial configuration can no longer sustain a large enough v_{min} and the algorithm must "accept" a less HC-beneficial configuration.

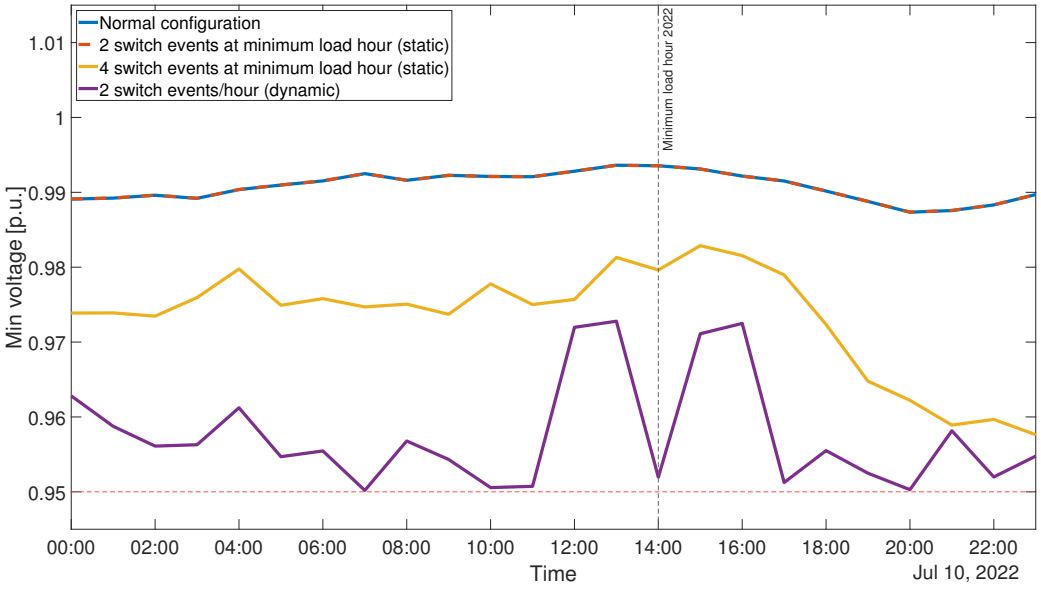

Figure 4.9: *Graph of the minimum voltage in the grid during the minimum load day, with DG placed at node N128 and production at maximum HC. The normal and $K = 2$ configuration curves (red and blue) overlap each other, suggesting that the minimum voltage occurs at the same node for these. The $K = 4$ configuration diverges from this and has a lower minimum voltage. The dynamic reconfiguration creates topologies with minimum voltages close to the lower limit, suggesting that actively striving towards maximizing DG power injection at one node makes the grid more vulnerable to drops in voltage at other nodes.*

The disadvantage of lower v_{min} during generation can be confirmed by looking at figure 4.10, which again shows v_{min} for the same configurations, but now with the voltage found by running PF with the *production removed* from the DG node. The $K = 0$ and 2 configurations have their v_{min} unchanged, showing that their respective robustness does not rely on the production at the DG node. The $K = 4$ and dynamic v_{min} curves on the other hand exhibit a drop in voltage below 0.95 p.u. There is a correlation between the drop in v_{min} when production was active and when it vanishes.

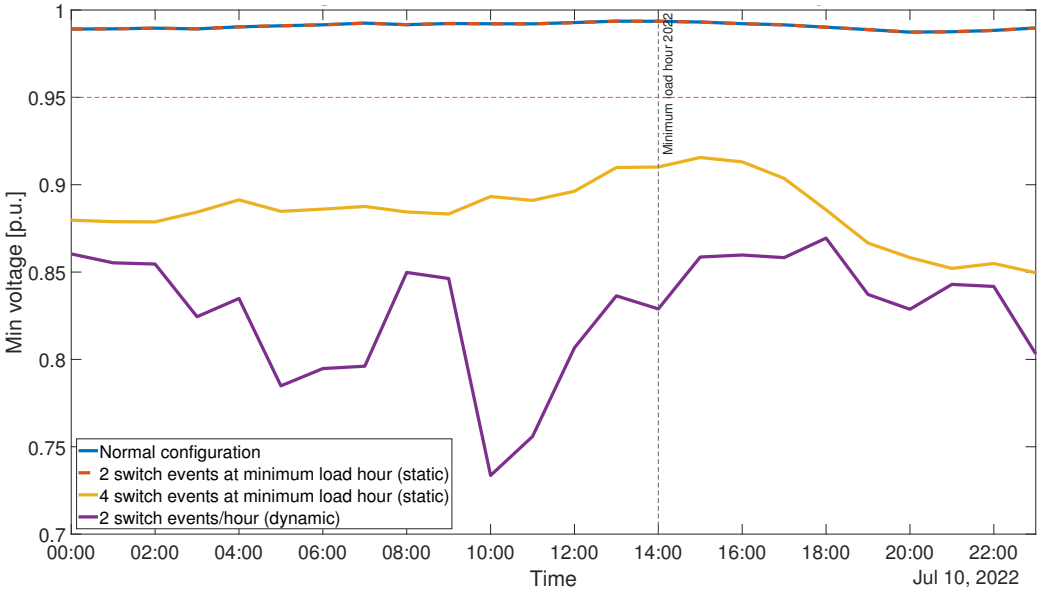

Figure 4.10: *Graph of the minimum voltage in the grid during the minimum load day, with all DG production removed. Configurations are kept the same as in figures 4.8 and 4.9, and a PF analysis was done to study the minimum voltage of the configurations if production was to fall away. The minimum system voltage for the normal and $K = 2$ configurations remain unchanged (overlapping), within operational limits. The $K = 4$ and dynamically created topologies on the other hand drop significantly below operational limits. This is probably because they were too specifically oriented towards maximizing DG power injection at node N128, with no other objective regarding e.g. robustness.*

For a final analysis of the single node case N128, we study how the found configurations perform on another day, this time during the maximum load day. The HC results of these simulations are found in figure 4.11. For this load scenario, the HC with the $K = 2$ configuration is still higher than with the normal configuration. The $K = 4$ configuration in turn was found to be infeasible during the maximum load day, meaning that there was no level of DG at node N128 the OPF algorithm could find that kept the system within operational limits. Again, the results indicate that what is optimal at one time may not be optimal (or even feasible) during other times. The dynamic reconfiguration starts with the $K = 2$ configuration and performs two switch events per hour, performing well. By comparing figure 4.11 to 4.8, it can be seen that the HC at node N128 is higher during the maximum load day than the minimum load day. A minimum voltage analysis has not been made for the maximum load day. Moreover, the following multi node generation scenarios will not include a HC analysis of the maximum load day.

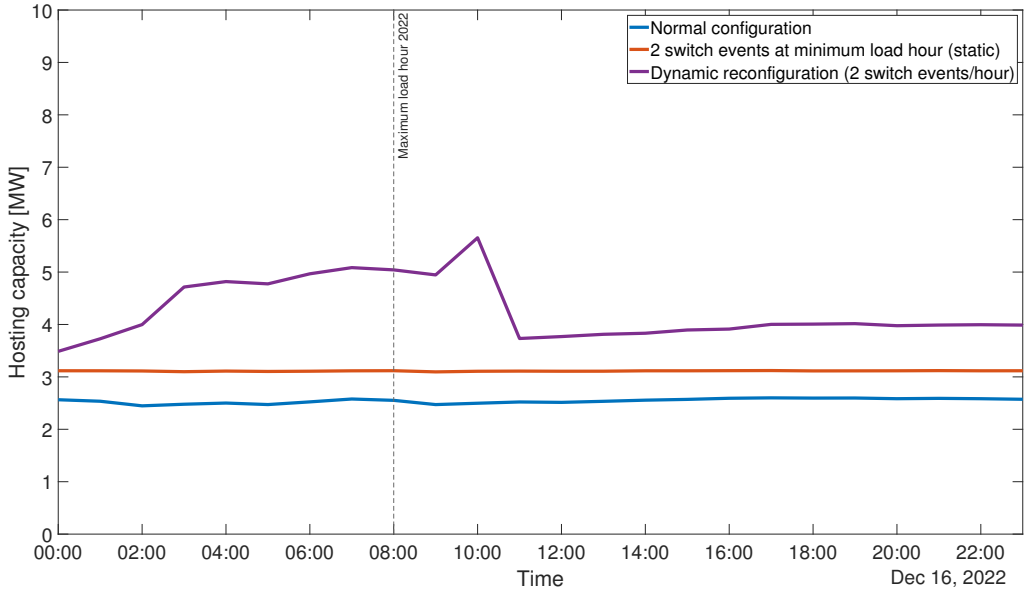

Figure 4.11: *Graph of the amount of generation that the grid can absorb (snapshot HC) at node N128 during the* ***maximum*** *load day. The static configurations (from the minimum load hour) were held constant, and the load was varied in accordance with the maximum load day. The dynamic case was started with the $K = 2$ configuration from the minimum load day, thereafter allowing two switch events every hour. The $K = 4$ configuration from the minimum load day was found to be infeasible under the load conditions of this day. It can be seen that the HC at node N128 during the maximum load day is higher or equal to the HC during the minimum load day for the same static configurations, further justifying the choice to optimize based on the minimum load hour.*

4.3.2 Multiple node – Double generation scenario

In the double generation scenario, twice the currently installed generation capacity is added to each node which has production today. In this scenario, the large difference is that there is (variable) p^G at several hundred nodes, compared to previous result sections where there has only been p^G at a single node at the time. The simulations are based on net load data, thus the HC should still be interpreted as additional HC from today. The HC reconfiguration results for the minimum load hour, as well as the topologies, can be seen in figure 4.12.

Figure 4.13 presents the HC for the static configurations created using this generation setup applied at the minimum load hour, along with a dynamic reconfiguration with two allowed switch events per hour. The total production capacity is $74.5 \times 2 = 149$ MW (production from Örtoftaverket is included here), and the DG injections (snapshot HC) in the simulations range from 125 MW to 137 MW, meaning that production is slightly curtailed. In figure 4.13, it can be seen that the reconfiguration with $K = 2$ created a topology with barely any increase in HC from the normal configuration, suggesting that with only two switch events, there are no configurations significantly better suited to this generation scenario. If four switch events are allowed, a slight improvement in HC of about 1-2 MW throughout the day can be seen. A similar improvement is given by the dynamic reconfiguration. Note that the y-axis in this case does not start at zero.

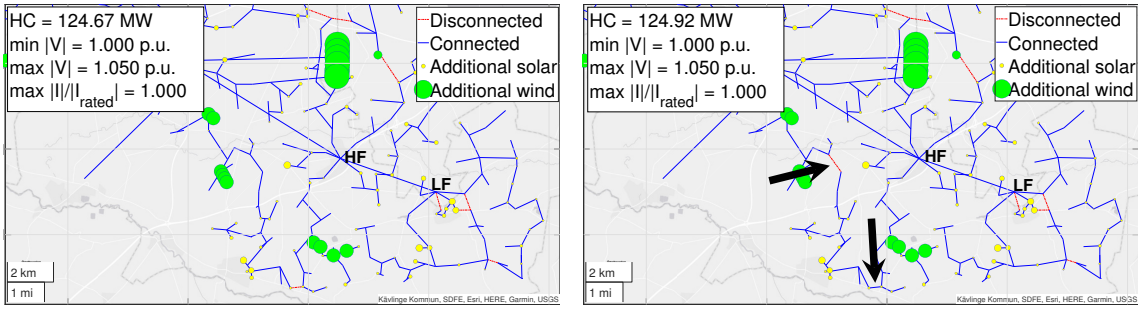

(a) Normal topology. *(b) Topology after 2 switch events.*

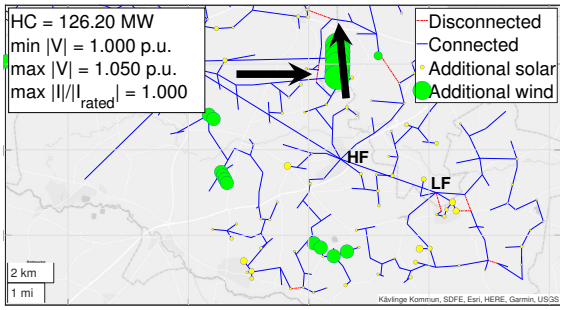

(c) Topology after 4 switch events.

Figure 4.12: *Maps showing the reconfigurations done in the double generation scenario. When only two switch events are allowed, a sectionalizing line and a tie line far out on the feeder southwest of HF (middle of figure) are switched, causing only a small increase in HC. When four switch events are allowed, the switch events instead occur close to the largest wind production cluster in the figure, causing an increase in HC of about 1.5 MW. Here as well there are two switch events not visible within this frame. Both current and voltage limits are reached in all cases, and the minimum voltage is high – indicative of a large amount of DG connected to the system.*

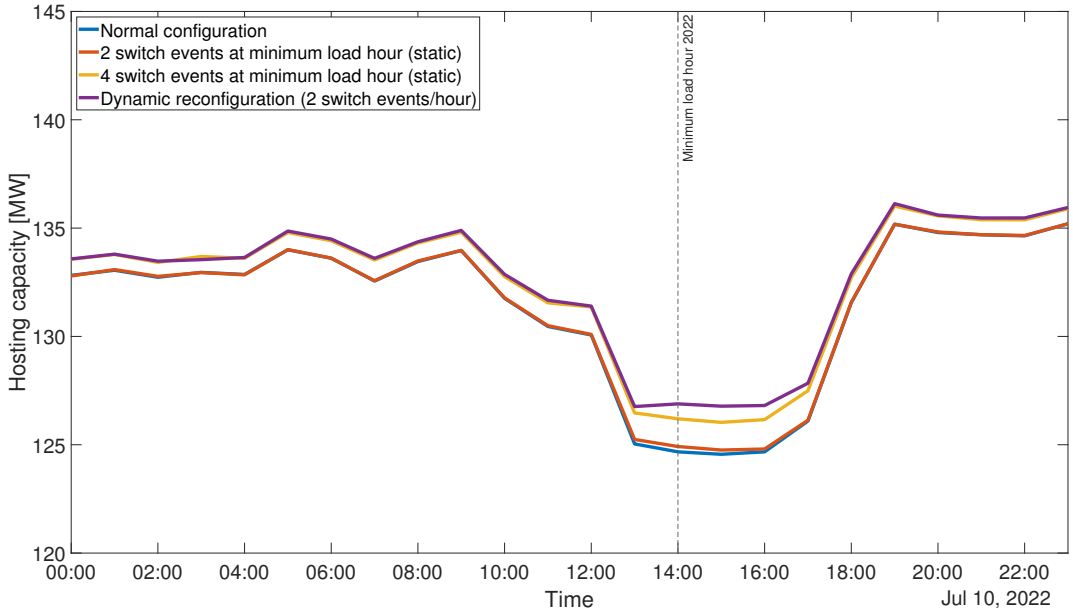

Figure 4.13: *Graph of the amount of production that the grid can accept (snapshot HC) during the minimum load day, with DG placed at all nodes with currently installed generation and twice the installed capacity of today. The blue, yellow and red curve are static configurations held constant throughout the day while the load was varied according to hourly data. The purple curve represents dynamic reconfiguration with two switch events allowed every hour. There is little to no significant increase in HC after reconfiguration, both at the minimum load hour and throughout the day. The dynamic operation performs very similar to the $K = 4$ configuration. The dip in HC around the minimum load hour is in line with the theory regarding the minimum load hour being the most HC limiting.*

Studying the minimum voltage in the system, v_{min}, for the various configurations throughout the day, which is done in figure 4.14, gives some further insight to the dynamic reconfiguration. For all static configurations, v_{min} is the same throughout the day, but for the dynamic reconfiguration, the voltage drops around the minimum load hour. This occurs after a switch event where a feeding line from the primary substation SP is opened. This new configuration leads to a very small further increase in HC compared to that given by the static $K = 4$ configuration, but this gain is only maintained for about three hours. After that, the HC returns to being essentially equal to that of the $K = 4$ configuration, but v_{min} does not return to its former level. It is still maintained within operational limits by the R-OPF algorithm, but as seen previously, this low minimum voltage indicates less robustness and risk of falling outside operational limits if load or generation is altered.

Given this information, keeping the static $K = 4$ configuration is preferable to the dynamic operation, even though the latter momentarily provides slightly higher HC. Given the minimum voltage at the end of the day, it is also likely that the dynamic reconfiguration would soon become limited by the lower voltage limit, leading either to reduced HC or infeasibility.

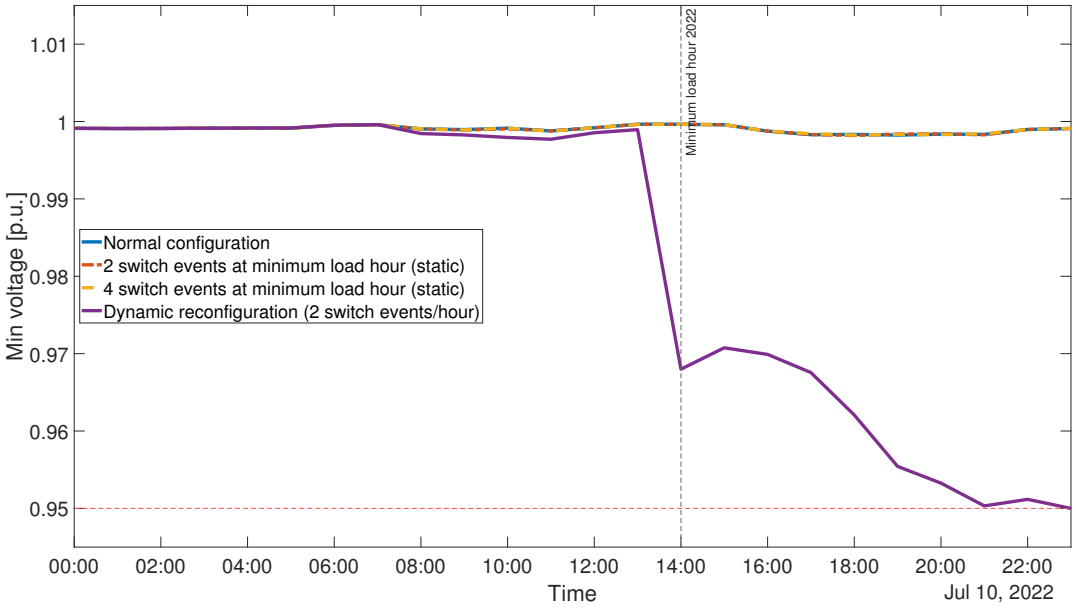

Figure 4.14: *Graph of the minimum voltage in the grid during the minimum load day, with DG placed at at all nodes with currently installed generation. With all static configurations, the minimum voltage in the network is kept high throughout the day. The dynamic operation, however, leads to a dip in voltage around the minimum load hour, which is never recovered. This occurs together with a small temporary increase in HC for the dynamic reconfiguration compared to the $K = 4$ configuration (see figure 4.13). Since the gain is small and short-lived, and the drop in voltage is negative for system robustness, this can be seen as an example of the unreliable nature of dynamic reconfiguration with this approach.*

4.3.3 Multiple node – Wind scenario

The wind scenario consists of 21 DG nodes with 2 MW installed capacity each, as described in section 3.5.3, placed according to figure 3.9. This contributes with a total capacity of 42 MW. The accepted DG injections are in the range of 20 to 25 MW according to figure 4.16, implying that the DG is significantly curtailed.

The reconfigurations executed when the R-OPF was run with the minimum load hour scenario and the wind generation setup can be seen if figure 4.15. The changes in topology occur in the bottom right corner of the map, near LF. The first pair of switch events is used to disconnect a line between two generators within a small cluster of four wind turbines. This can be seen in the bottom right of the subfigures. This switch event splits the wind cluster in two pairs, and places the turbines on different radials instead of having them all connected to the same one. This seems a very reasonable action for increasing the HC, since the power can then be shared between two paths instead of just one. The effect is an increase in HC of 1.61 MW. If a second pair of switch events is allowed, the algorithm switches between two adjacent lines close to LF. This has very little effect on the HC, which only increases with 0.11 MW. The slight increase is presumably due to the redistribution of loads to a feeder with DG, making conditions slightly more favorable for DG injection on that feeder.

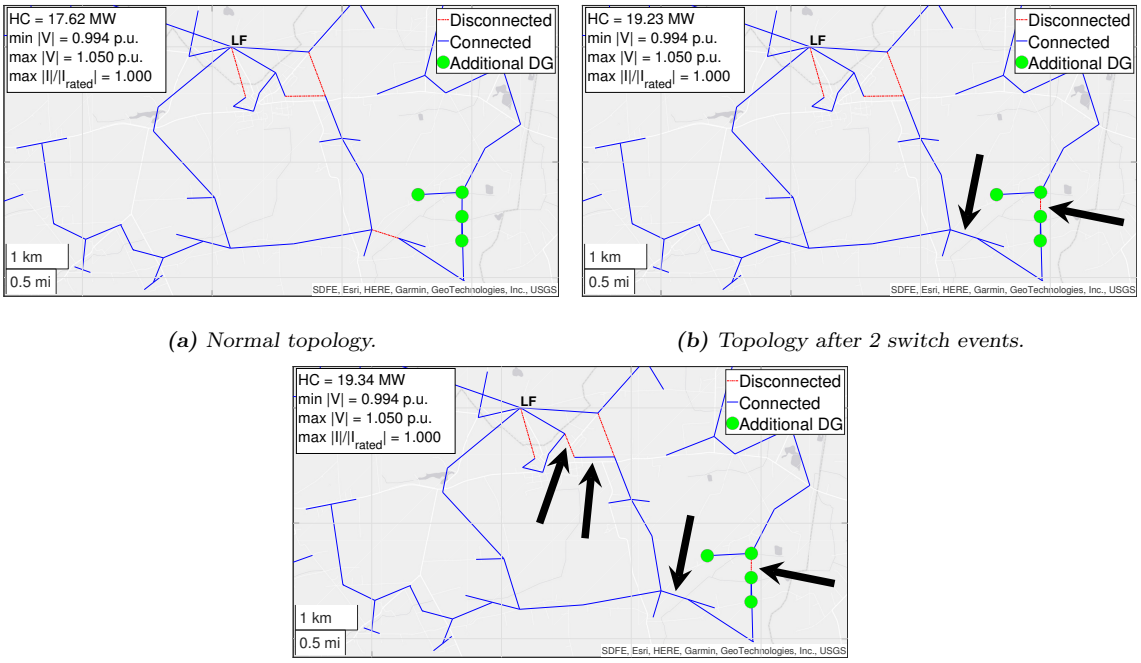

(a) *Normal topology.*

(b) *Topology after 2 switch events.*

(c) *Topology after 4 switch events.*

Figure 4.15: *Images zoomed in at the southeastern corner of the Eslöv distribution network, around some of the nodes with added DG (see figure 3.9). The subfigures show the normal configuration and the changes in topology after two and four switch events are performed. In all cases, both voltage and current limits are reached. In (b), the first pair of switch events results in the disconnection of a line between two generators within a small cluster of four wind turbines. This switch event splits the wind cluster in two pairs, and places the turbines on different radials instead of having them all on the same one. This seems a very reasonable action for increasing the HC, since the power can then be shared between two paths instead of just one. The effect is an increase in HC of 1.61 MW. In (c), the second pair of switch events causes a change closer to the LF distribution substation. This leads to a slight redistribution of loads, but only increases HC with an additional 0.11 MW.*

The increase in HC from the $K = 2$ configuration, and the slight additional increase from $K = 4$, can be seen throughout the minimum load day in figure 4.16. The curves follow each other steadily, suggesting that the new configurations are stable. This is supported by the v_{min} results in figure 4.17, where the minimum system voltage is equal and far from the lower limit during all hours of the day for all three static configurations. This indicates that v_{min} is located at the same node in all three cases and throughout the day, and that this node is not affected by the reconfigurations.

More remarkable are the results from the dynamic reconfiguration. This approach manages to find topologies with better HC than the static for all hours up until 18:00, after which it can no longer find any feasible configurations (the steep drop to zero in the graph). This appears to be due to an abrupt drop in voltage at 16:00, that was not recovered by the algorithm. Upon inspection of which reconfiguration caused the drop in voltage, it was determined that the algorithm had disconnected the HV line between Eslöv S and SP, in order to allow activation of a line further out in the network. This was apparently beneficial to the HC at the times 16:00 and 17:00 as can be seen in the graph. Nevertheless, when the load scenario changed, this led to a drop in voltage below the operational limit that no two switch events with subsequent generation could stop. Events such as this could perhaps be avoided by implementing safeguards to the algorithm, that prohibit certain essential lines from being disconnected, a concept which is discussed further in chapter 5.

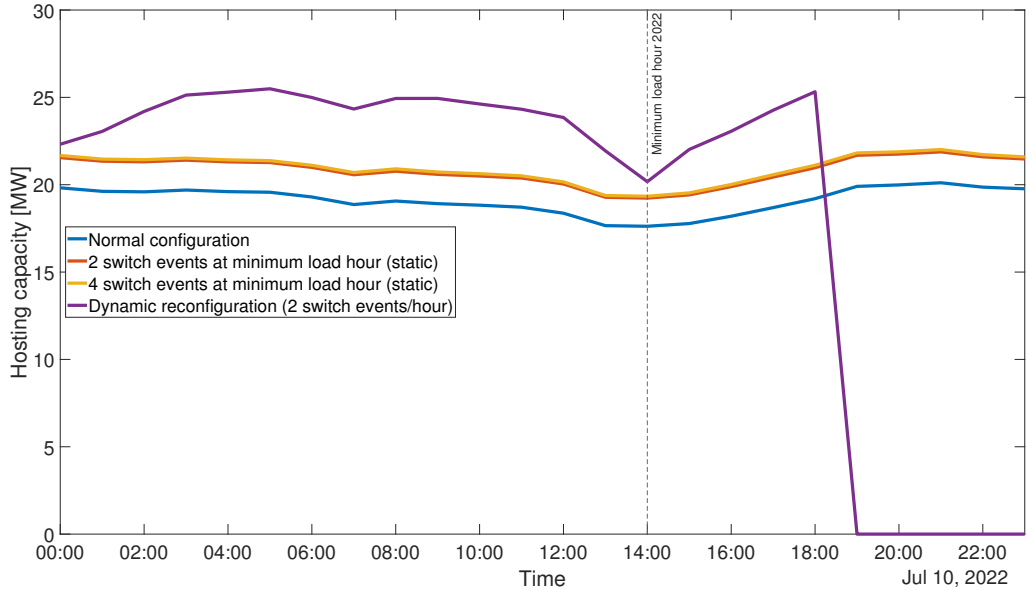

Figure 4.16: *Graph of the amount of production that the grid can accept (snapshot HC) during the minimum load day, with DG placed at 21 nodes of 2 MW/node in the rural area (according to the wind scenario). The blue, yellow and red curve are static configurations held constant throughout the day while the load was varied according to hourly data. The purple curve represents dynamic reconfiguration with two switch events allowed every hour. There is some significant increase in HC after reconfiguration with $K = 2$, but no further significant increase with $K = 4$. The dynamic operation causes a further HC enhancement, which is maintained (although with some erratic behavior) until 18:00, after which no feasible solution can be found by the algorithm.*

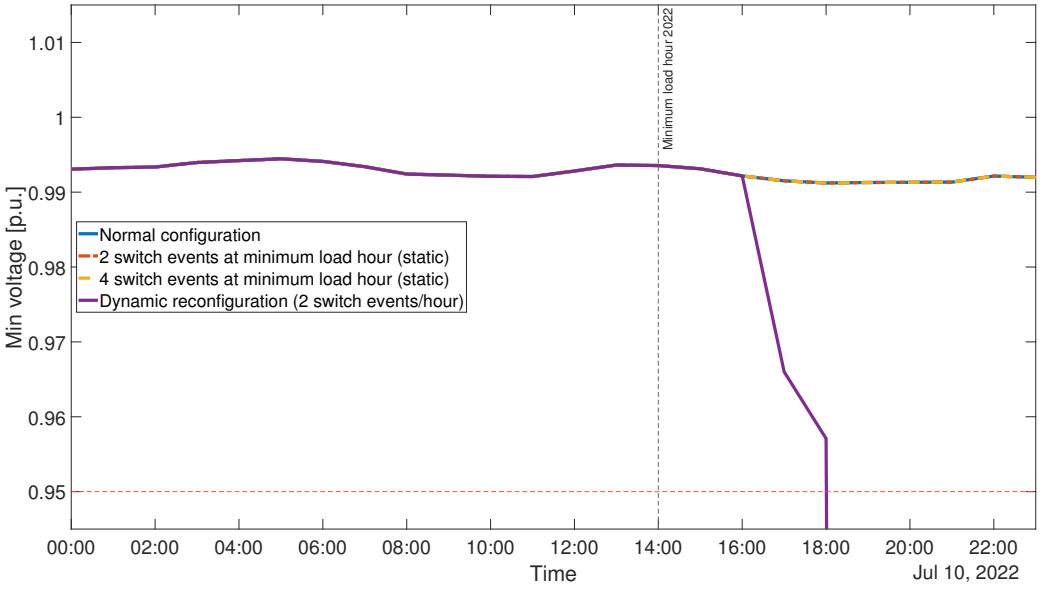

Figure 4.17: *Graph of the minimum voltage in the grid during the minimum load day, with DG placed at 21 nodes of 2 MW/node in the rural area (according to the wind scenario). All static configurations exhibit the same v_{min} level throughout the day, meaning that the reconfigurations have probably not affected the node where the v_{min} occurs. The dynamic reconfiguration curve follows the static until 16:00, then it drops sharply. Since the drop provides an increase in HC, this drop continues until 18:00. After this, it is assumed that no reconfiguration can be performed with only two switch events that returns a feasible solution for the load scenario at the time.*

4.3.4 Multiple node – Solar scenario

Simulations were initiated for a rooftop solar scenario, where DG was placed at all 112 urban nodes of 1 MW/node within urban areas. The simulations were supposed to be presented in the same manner as in sections 4.3.1-4.3.3. However, these simulations were never completed due to them being too time-consuming. With this generation setup, running through the 24 hourly load scenarios with one static configuration took more than four days to complete, which was deemed too long to continue with the other configurations or dynamic reconfiguration. Previous scenarios had taken a few hours to simulate.

The underlying reason to why this optimization took significantly longer to complete than the others with similar setup is unknown and difficult to investigate, but educated guesses can be made. An initial hypothesis was that the large number of nodes with DG was the main factor, causing the search space of the optimization to grow larger which would make the computation slower. There are 112 nodes classified as urban, which all have DG in this case, so it seems reasonable that this case would take longer to run than the wind scenario with only 21 DG nodes. However, the double generation scenario had DG placed at 262 nodes, and those simulations were completed within reasonable time. This makes it unlikely that it is simply the number of modeled DG units that causes the increase in runtime.

Our leading hypothesis is that the long runtime is connected to the DG locations. In the solar case, many nodes with production are connected in close proximity to each other, which is not the case (at least not to the same extent) in the other multiple node generation scenarios. In addition, the modeled PV units had large installed capacities, resulting in the need for curtailment at many nodes. If two DG nodes are placed far from each other, on completely separate radials, their allowed production (HC) will only be determined by the limits on their respective lines. If they are on the same radial however, their total production will be limited, and consequently the production of one unit will be in conflict with the production of the other. Having a large number of nodes with production in a small area, most of which need to have their production curtailed, may possibly increase the search space of the optimization, since many of the variables are in clinch with each other.

Chapter 5

Discussion

In this chapter, general conclusions and traits from the results are outlined. In section 5.1, general aspects will be presented. Section 5.2 outlines potential improvements of the R-OPF algorithm, the aim being to make it more applicable to real networks and capture realistic network characteristics with higher accuracy. Finally, section 5.3 will outline potential future work on the topic – things that were not studied in this thesis but would be interesting to look at in future studies.

5.1 Conclusions

Based on the literature review and the case study in this thesis, reconfiguration optimization in general, and the R-OPF algorithm in particular, shows promise when it comes to enhancing the HC in distribution networks. In contrast to reinforcement or expansion of the grid, reconfiguration comes at little or no cost, making it a very attractive option for DSO:s. Distribution systems are traditionally designed to handle load only, and when DG is expanding at scale, turning consumers into prosumers, it is well worth reviewing the present grid configuration.

The benefit of reconfiguration is highly dependent on where and how much DG is added. Consequently, it is not possible to give a direct answer on how much HC can be enhanced by reconfiguration. As can be seen in the system analysis, the HC can increase with as much as 212% in single node cases if four switch events are allowed, while the median increase in all single node cases is only 11%. If DG is added en masse throughout the system, such as in the double generation scenario, there is little significant increase in HC to be gained from reconfiguration, at least not in this case study. This is likely because the grid is congested in several places or bottlenecks, making reconfiguration a zero-sum game. An analogy to this is that there is no way for a (car) commuter to avoid traffic jams if all routes are congested. This illustrates that the physically existing infrastructure has limitations and that there are cases when expansion or reinforcement of the grid, such as building additional lines, is the only remaining option. The HC enhancement from reconfiguration in the wind scenario lies somewhere in between the double generation scenario and the most beneficial single node cases. In this case, DG is added to a handful of rural locations and the R-OPF algorithm identifies a specific reconfiguration in the vicinity of LF that turns out to be particularly advantageous.

An important question is how the R-OPF algorithm can be applied or implemented in practice by a DSO. Here, one of the main takeaways is that the R-OPF can be of great use when someone applies for connecting DG to the grid. Applications for permission to connect DG are generally handled by DSO:s on a case-by-case basis [17] and fortunately, the R-OPF is suitable for this particular judgment. With the R-OPF, the DSO can assess not only the HC at a specific node with the present configuration, but also find if another static configuration is more advantageous and can be applied straight away. An example of this can be seen in the N128 single node case or the wind scenario, where additional HC:s of several MW can be instantly realized by simply switching to new static configurations (with seemingly little or no negative impact on voltage profile). The R-OPF can be implemented in a human-controlled decision support system to see, on a case-by-case basis,

if there is an alternative configuration of the grid that has been overlooked. On the same note, the R-OPF could be used to see which secondary substations should have sectionalizing switches installed. The R-OPF at present does not take into account where switching possibilities actually exist today, thus the results can be interpreted as "perform switch event here", regardless of the existence of a switch. Performing reconfiguration when switching possibilities exist is virtually free of charge. Installing switches is also generally a cheaper option than reinforcing the grid with new lines. Since DSO:s are often obliged to eventually accommodate all installed DG in grid, there are likely economic profits to be gained from implementing the R-OPF in a decision support system.

For dynamic reconfiguration to be implemented, the switching would need to be at least partly automatized. This in turn requires overcoming several obstacles regarding both the R-OPF algorithm and the physical grid. As previously mentioned, there is a clear trade-off between optimality and robustness. As the R-OPF algorithm is formulated at present, the optimization is performed based on a single snapshot in time, with predefined load and generation. Although this will indeed return the optimal HC at that specific time, there is a risk that the configuration returned is unreliable and that even small changes to load or generation will return a scenario where the grid does not operate within limits. As it presently stands, the robustness of all returned configurations will have to be checked and verified before they are applied in practice. How the robustness of the configurations can be dealt with from an optimization perspective is discussed further under potential improvements. From a grid perspective, implementing dynamic reconfiguration would first of all require accurate real-time metering of the net load at all nodes in the system. Moreover, all switches would require remote control. A control system that switches back to the normal configuration if a large DG unit falls away could also be of great use. Finally, as the grid in Eslöv (and many others) is operated today, loads are sometimes required to be disconnected momentarily in order for switching to be possible. For a dynamic reconfiguration scheme to be viable, the implementation of on-load switching would be a necessary precondition. This is not infeasible, but would require some further investments.

In the future, the operational topology of MV distribution networks might as well be meshed, similar to the operation of HV transmission networks. This is more a question of cost and how conservative the DSO:s are, rather than a physical impossibility. It begs the question whether it is more realistic to implement dynamic reconfiguration, performing switch events on an hourly basis, than to transition to meshed operation. Both methods are likely to require major changes to the protection system. Meshed operation has the advantage that all infrastructure is utilized simultaneously, thus increasing the HC more than any possible radial configuration.

5.2 Potential algorithm improvements

As previously mentioned, the robustness of returned configurations has been a concern throughout this project. The algorithm optimizes based on a single snapshot in time and generally returns long radial feeders to accommodate more DG at that time. Adjusting the objective function or constraints in the R-OPF algorithm to make sure the newly found configurations are robust in case of load and generation changes would make the configurations more reliable. This in turn would likely improve a DSO:s willingness to implement the algorithm in a real system.

One way to achieve more robust solutions could be to implement stricter constraints on the switch status of a number of lines, for example defining some important lines as always connected. It is for example very unlikely that the DSO is interested in disconnecting the main feeders from SP and ÖP to the distribution hubs MF, HF and LF (as the optimization algorithm does in some scenarios), or from the infeed station at Eslöv S. Implementing this in the algorithm should be possible to do with relative ease.

Two other, more intricate ways to achieve robust solutions could be to implement multi-objective optimization or stochastic programming. Multi-objective optimization could be implemented by weighting the current objective function (snapshot maximization of HC) against some penalty func-

tion that takes into account how much the operational limits are violated in some other defined load and generation scenario. Stochastic programming is a framework that contrasts deterministic optimization in the sense that some variables are allowed to be unknown, following some probability distribution. The natural unknowns in this case would be load and generation. Both multi-objective optimization and stochastic programming would require rather major changes to the R-OPF algorithm as it currently stands.

Going forward, alternative related objective functions deserve further investigation. The algorithm in its current form has maximization of DG input to the grid as objective function:

$$\underset{\nu,\ell,p^G,q^G,P,Q,\pi,\alpha}{\text{maximize}} \sum_{i\in\mathcal{N}} p_i^G$$

Another objective function, that is also highly interesting to a DSO, is minimization of active power losses. A third alternative, that implicitly combines the two just mentioned, is minimization of the net import from the external regional grid (through the slack bus). If we consider all generation in the distribution network to be DG and all loads to be fixed, minimizing the net import is equivalent to maximizing DG with the deduction of losses ($DG - Losses$):

$$DG + Net\ import = Loads + Losses$$

$$\min\left(Net\ import\right) = \max\left(DG - Loads - Losses\right) = \max\left(DG - Losses\right) - Loads$$

From both the DSO and the consumer viewpoint, this objective function has several benefits compared to the current one. Including losses in the objective function makes it more adequate from a socioeconomic perspective – e.g. an additional 0.1 MW injection of DG to the grid is not very rational if this implies an additional 1 MW in grid losses. From an algorithm viewpoint, it is also an attractive adjustment since the net import from the external grid is simply the power flow through the slack bus, P_0. Either P_0 could be added to the optimization variables (not included at present) and the objective function would be:

$$\underset{\nu,\ell,p^G,q^G,P,Q,\pi,\alpha}{\text{minimize}} P_0$$

Alternatively, since P_0 is not included in the optimization variables, the same objective function could be formulated as:

$$\underset{\nu,\ell,p^G,q^G,P,Q,\pi,\alpha}{\text{minimize}} \sum_{i\in c(0)} P_i = \underset{\nu,\ell,p^G,q^G,P,Q,\pi,\alpha}{\text{minimize}} \sum_{i\in\mathcal{N}} \pi_{0i} P_i$$

Possibly, this could allow R-OPF runs of systems with DG at a larger number of buses, such as the urban solar scenario, in reasonable time. This because the current objective function, which has a large number of variables (p_i^G) when there is a large number of DG units, is replaced with an objective function with only one or a few variables (P_i) related to the slack bus. However, this has not been looked into further and is a mere speculation.

Other adjustments that would make the optimization more applicable in reality would be to implement constraints on the amount of reactive power that can be imported from the external grid, and constraints on the apparent power rating of the transformers in the distribution substations. A final useful improvement to the R-OPF algorithm would be to implement the PV bus type, in addition to the PQ and slack type, to represent voltage control within the network. Many distribution networks have some sort of voltage control within the network, e.g. tap-changing transformers or capacitor banks, that will affect the solution of the PF. Voltage control is also an important HC enhancement technique, so it would be useful if it could be implemented in combination with reconfiguration optimization. Assigning the slack bus type to all substations with voltage control and solving for separate subsystems would not work, since the voltage controlled substations are likely to share secondary substations that can be fed from either of them. With reconfiguration, nodes can switch from belonging to one voltage controlled substation to another. This is for example the case with many of the nodes connected to SP and ÖP. There is usually only one distinct slack bus, in our case the feed-in substation Eslöv S.

5.3 Future work

A lot of time in this project was spent building the Matpower case model of the Eslöv network from scratch, using raw data from Kraftringen in Excel format. Understanding and implementing the R-OPF algorithm developed by Sou also took some time. This consequently took time from the analysis of reconfiguration as a HC enhancement technique. Since the problem is very broad, there are numerous other key figures that could have been analyzed, and countless scenarios for which optimization could have been run.

Reconfiguration as a HC enhancement technique has in this thesis been analyzed using a deterministic approach, based on one or a couple of worst-case scenarios such as the minimum load hour in 2022. Naturally, it is of interest to know if the found configurations are robust enough and if the worst-case scenario on a system level is also the most HC limiting in specific parts of the grid. For future work, using a probabilistic approach would be valuable. It would also be preferable to take a longer time span into account than only the net-load data from a single year, and to differentiate the worst-case scenario based on location in the grid.

Some parameters required for the model were unknown and thus kept constant (at reasonable values) throughout the project. This was for example the case for the lower power factor limit of the generators/inverters, pf_{min}, which was set to 0.9 in all cases, and the reactive loads, q^L, which were kept at 1% of the active loads, p^L. This however makes the impact of these parameters on the HC difficult to gauge. Varying these parameters to see their influence on the HC would be a natural research question for future work.

On the same note, a comparison or compatibility analysis of different HC enhancement techniques, including reconfiguration, would be an interesting research objective for a follow-up study. A comparative study could for example be a quantitative study of which HC enhancement technique has the highest potential. A compatibility analysis could focus on possible competition or synergy effects between the techniques. A HC enhancement technique that at least partly competes with reconfiguration is voltage control, using e.g. tap changing transformers or capacitor banks. With distributed voltage control in the grid, the need for reconfiguration to avoid breaching voltage constraints is less urgent. On the other hand, distributed voltage control could help make new configurations more robust. With voltage control along the long radials that the R-OPF returns, the system is less susceptible to sudden drops in voltage in case DG falls away. Another HC enhancement technique that should work well in combination with reconfiguration is active power curtailment. With curtailment, more DG can be installed in the grid and with reconfiguration, more DG can be injected. Overall, reconfiguration should be compatible with most HC enhancement techniques. Changing the topology at times does not hinder installing energy storage, capacitor banks, new lines, etc.

A research objective which was initially included in this thesis but had to be discarded, was using the R-OPF algorithm as decision support when planning for an expansion or reinforcement of the grid. By adding additional tie lines to the model, the R-OPF algorithm could have been run to see where added lines would be of most use. This problem would have introduced even more degrees of freedom, as it would not only involve freedom of choice in the addition of DG, but also in the addition of new tie lines with a continuous range of possible impedances and rated currents. The cost of the new lines would also be an important factor to take into account. All in all, this is an intricate and relevant problem, but complex enough to be a separate study.

A final issue that would be interesting for future studies is the fairness aspect of reconfiguration (and HC control over all). To exemplify, the HC at a given node can vary largely depending on how many other DG units are connected in the area, and this becomes an even larger issue when reconfiguration comes into play. Should the DSO have the right to decrease the HC at a given node, and potentially curtail DG there, to increase the HC more on another, thus increasing the total possible production? Should the configuration that gives the highest total HC in the grid always be prioritized? In this study, we have defined the net loads ($p^L - p^G$) and added only

additional DG as variable, thus defining existing DG as a fixed parameter. This can be seen as the most just approach, since DG producers that already have been granted access to the grid naturally do not want to be subject to curtailment. An alternative approach would be to define only the actual loads p^L as fixed, and add both existing and additional DG as variable. This would have returned solutions with a higher total HC in the system, but existing DG units would on the other hand likely be curtailed.

Bibliography

[1] National Renewable Energy Laboratory. Advanced hosting capacity analysis. `www.nrel.gov/solar/market-research-analysis/advanced-hosting-capacity-analysis.html`, 2019. Accessed: 2023-04-26.

[2] K.C. Sou and K. Girón. Joint Renewable Generation Maximization and Radial Distribution Network Reconfiguration. In *2022 IEEE PES Innovative Smart Grid Technologies - Asia (ISGT Asia)*, pages 16–20, 2022.

[3] K. Rauma, F. Cadoux, N. Hadjsaid, A. Dufournet, C. Baudot, and G. Roupioz. Assessment of the MV/LV on-load tap changer technology as a way to increase LV hosting capacity for photovoltaic power generators. In *CIRED Workshop 2016*, pages 1–4, 2016.

[4] D. Caples, S. Boljevic, and M.F. Conlon. Impact of distributed generation on voltage profile in 38kV distribution system. In *2011 8th International Conference on the European Energy Market (EEM)*, pages 532–536, 2011.

[5] B. Bletterie, S. Kadam, and J. Le Baut. Increased hosting capacity by means of active power curtailment. In *CIRED Workshop 2016*, pages 1–4, 2016.

[6] W. Sun and G.P. Harrison. Influence of generator curtailment priority on network hosting capacity. In *22nd International Conference and Exhibition on Electricity Distribution (CIRED 2013)*, pages 1–4, 2013.

[7] S. M. Ismael, S. H.E. Abdel Aleem, A. Y. Abdelaziz, and A. F. Zobaa. State-of-the-art of hosting capacity in modern power systems with distributed generation. *Renewable Energy*, 130:1002–1020, 2019.

[8] S. M. Mirbagheri, D. Falabretti, V. Ilea, and M. Merlo. Hosting Capacity Analysis: A Review and a New Evaluation Method in Case of Parameters Uncertainty and Multi-Generator. In *2018 IEEE International Conference on Environment and Electrical Engineering and 2018 IEEE Industrial and Commercial Power Systems Europe (EEEIC / I&CPS Europe)*, pages 1–6, 2018.

[9] V. Calderaro, A. Piccolo, and P. Siano. Maximizing DG penetration in distribution networks by means of GA based reconfiguration. In *2005 International Conference on Future Power Systems*, pages 6 pp.–6, 2005.

[10] P.C. Ramaswamy, P. Vingerhoets, and G. Deconinck. Reconfiguring distribution grids for more integration of distributed generation. In *22nd International Conference and Exhibition on Electricity Distribution (CIRED 2013)*, pages 1–4, 2013.

[11] A. Bayat, A. Bagheri, and R. Noroozian. Optimal siting and sizing of distributed generation accompanied by reconfiguration of distribution networks for maximum loss reduction by using a new UVDA-based heuristic method. *International Journal of Electrical Power & Energy Systems*, 77:360–371, 2016.

[12] F. Capitanescu, L. Ochoa, H. Margossian, and N. Hatziargyriou. Assessing the Potential of Network Reconfiguration to Improve Distributed Generation Hosting Capacity in Active Distribution Systems. *IEEE Transactions on Power Systems*, 30:346 – 356, 01 2015.

[13] W.M. Dahalan and H. Mokhlis. Network reconfiguration for loss reduction with distributed generations using PSO. In *2012 IEEE International Conference on Power and Energy (PECon)*, pages 823–828, 2012.

[14] H. Wang, J.S. Pan, T. Nguyen, and S. Weng. Distribution network reconfiguration with distributed generation based on parallel slime mould algorithm. *Energy*, 244:123011, 2022.

[15] R. Chidanandappa, T. Ananthapadmanabha, and H.C. Ranjith. Genetic Algorithm Based Network Reconfiguration in Distribution Systems with Multiple DGs for Time Varying Loads. *Procedia Technology*, 21:460–467, 2015. SMART GRID TECHNOLOGIES.

[16] M. Hormozi. Optimal Network Reconfiguration and Distributed Generation Placement in Distribution System Using a Hybrid Algorithm. *International Journal of Energy and Power Engineering*, 5:163, 01 2016.

[17] *Personal communication with Kraftringen.*

[18] R. A. Jabr, R. Singh, and B. C. Pal. Minimum Loss Network Reconfiguration Using Mixed-Integer Convex Programming. *IEEE Transactions on Power Systems*, 27(2):1106–1115, 2012.

[19] M. Aien, A. Hajebrahimi, and M. Fotuhi-Firuzabad. A comprehensive review on uncertainty modeling techniques in power system studies. *Renewable and Sustainable Energy Reviews*, 57:1077–1089, 2016.

[20] Svenska Kraftnät (in Swedish). Sveriges elnät. `https://www.svk.se/om-kraftsystemet/oversikt-av-kraftsystemet/sveriges-elnat/`, Dec 2022. Accessed: 2023-05-03.

[21] J. D. Glover, M. S. Sarma, and T. J. Overbye. *Power system analysis and design : Si Edition.* Cengage Learning, Stamford, CT, 5. edition, 2012.

[22] R. Sundin (in Swedish). *Elinstallationer. 3, Faktabok.* LiberLäromedel, 2 [rev.] edition, 1987.

[23] S. Stewart. *Distribution switchgear [electronic resource].* Institution of Engineering and Technology, London, 2008.

[24] O. Granhaug, K. Isaksen, F. Mekic, J. Holmlund, and M. Stefanka. Compact Secondary Substation in a Future Medium Voltage Distribution Network. In *21st International Conference on Electricity Distribution (CIRED 2011)*, 06 2011.

[25] T. Walla. Hosting capacity for photovoltaics in Swedish distribution grids. Master's thesis, Uppsala University, Department of Engineering Sciences, Solid State Physics, 2012.

[26] M.E. Baran and F.F. Wu. Optimal capacitor placement on radial distribution systems. *IEEE Transactions on Power Delivery*, 4(1):725–734, 1989.

[27] DIgSILENT Power Systems Solutions. Optimal Power Flow. `https://www.digsilent.de/en/optimal-power-flow.html`. Accessed: 2023-04-20.

[28] C. Long, J. Wu, L. Thomas, and N. Jenkins. Optimal operation of soft open points in medium voltage electrical distribution networks with distributed generation. *Applied Energy*, 184:427–437, 12 2016.

[29] Gurobi Optimization. Mixed Integer Programming (MIP) - A Primer on the Basics. `www.gurobi.com/resources/mixed-integer-programming-mip-a-primer-on-the-basics/`. Accessed: 2023-05-05.

[30] Matpower. About MATPOWER. https://matpower.org/about. Accessed: 2023-04-25.

[31] J. McDowell, R. Walling, W. Peter, E. Von Engeln, E. Seymour, R. Nelson, L. Casey, A. Ellis, and C. Barker. Reactive power interconnection requirements for PV and wind plants: recommendations to NERC. *Sandia National Laboratories*, 2 2012.

[32] Interstate Renewable Energy Council (IREC). Optimizing the Grid: Regulator's Guide to Hosting Capacity Analyses. `https://irecusa.org/resources/optimizing-the-grid-regulators-guide-to-hosting-capacity-analyses/`. Accessed: 2023-05-15.